Title Page

Allosteric Structural Alterations and Auto-regulation of Rab5 GEF Activity in Rabex5

Janelle Lauer[1], Alice Cezanne[1], Giambattista Guaitoli[2], Francesco Raimondi[3,4], Marc Gentzel[5], Vikram Alva[6], Michael Habeck[7,8], Marius Ueffing[9], Andrei Lupas[6], Christian Johannes Gloeckner[2,9], and Marino Zerial[1]

[1]Max Planck Institute of Molecular Cell Biology and Genetics, Dresden, Saxony 01307, Germany

[2]German Center for Neurodegenerative Diseases, Otfried-Müller-Str. 23, 72076 Tübingen, Germany.

[3]Bioquant, Heidelberg University, Im Neuenheimer Feld 267, 69120, Heidelberg, Germany

[4]Heidelberg University Biochemistry Centre (BZH), Im Neuenheimer Feld 328, 69120, Heidelberg, Germany

[5]Molecular Analysis-Mass Spectrometry Center for Molecular and Cellular Bioengineering, Technical University Dresden, Tatzberg 41, 01307 Dresden

[6]Max-Planck-Institute for Developmental Biology, Max-Planck-Ring 5, 72076 Tübingen, Germany.

[7]Statistical inverse problems in Biophysics, Max Planck Institute for Biophysical Chemistry, Am Fassberg 11, 37077 Göttingen

[8]Felix Bernstein Institute for Mathematical Statistics in the Biosciences, University of Göttingen, Goldschmidtstrasse 7, 37077 Göttingen

[9]University of Tübingen, Institute for Ophthalmic Research, Center for Ophthalmology, Elfriede-Aulhorn-Str. 5-7, 72076 Tübingen, Germany

Abstract

Intracellular trafficking depends on the function of Rab GTPases, whose activation is regulated by guanine exchange factors (GEFs). The Rab5 GEF, Rabex5, was previously proposed to be auto-inhibited by its C-terminus. Here, we studied full-length Rabex5 and Rabaptin5 proteins as well as domain deletion Rabex5 mutants using hydrogen deuterium exchange mass spectrometry. We generated a structural model of Rabex5, using chemical crosslinking mass spectrometry and integrative modeling techniques. Our results are inconsistent with the previous model of auto-inhibition. By correlating structural changes with nucleotide exchange activity for each construct, we uncovered new auto-regulatory roles for the Ubiquitin binding domains and the Linker connecting those domains to the catalytic core of Rabex5. Our results suggest a more complex auto-regulation mechanism than previously thought and imply that Ubiquitin binding serves not only to position Rabex5 but to also control its Rab5 GEF activity through allosteric structural alterations.

Introduction

Small GTPases were identified almost 40 years ago and the superfamily has grown to include more than 70 human members (Cherfils & Zeghouf, 2013, Rojas, Fuentes et al., 2012, Shih, Papageorge et al., 1980, Wittinghofer & Vetter, 2011). These proteins regulate an array of activities such as cell growth and differentiation, organelle biogenesis, intracellular transport, cytoskeletal organization, and cell division (Cherfils & Zeghouf, 2013). Activation and deactivation of small GTPases are controlled by cycling through inactive GDP-bound and active GTP-bound states. These cycles are regulated by guanine nucleotide exchange factors (GEFs), and GTPase activating proteins (GAPs) (Bos, Rehmann et al., 2007, Zerial & McBride, 2001). In addition, most small GTPases carry a C-terminal lipid modification and variable C-terminal amino acid sequences. This provides a means of membrane association and additional layers of control such as extraction and insertion into specific membranes. Following insertion into the proper membrane and GDP/GTP exchange by an appropriate GEF, the active GTPase can associate with effector molecules mediating biological activity and protecting it from membrane extraction by guanine nucleotide dissociation inhibitors (GDIs) (Cherfils & Zeghouf, 2011). The activity of GEFs is therefore of primary importance for the regulation of localization and downstream function of small GTPases. Thus, it is not surprising that the GEF activity is subjected to a tight and complex control (Cherfils & Zeghouf, 2013). Most GEFs follow the unifying mechanism of making contacts in switch1 and switch 2 regions near the GTPase nucleotide binding pocket to facilitate nucleotide exchange. Regulation of this activity includes, but is not limited to, multiple allosteric activation sites as well as multiple domains, some of which are involved in auto-regulation. For example, one of the best studied GEFs is Sos, which activates Ras proteins. Sos is auto-regulated allosterically by the C-terminal proline-rich domain and the N-terminal Histone, Dbl-homology, and Rem domains (Hall, Yang et al., 2002, Lee, Low-Nam et al., 2017, Sondermann, Soisson et al., 2004, Yadav & Bar-Sagi, 2010).

Convergent evolution has created many structurally unrelated domains or modules capable of GEF activity [reviewed in (Cherfils & Zeghouf, 2013)]. For the Rab family, which comprises the largest number of members and regulates membrane transport and organelle biogenesis, the list includes the DENN (differentially expressed in normal and neoplastic cells)

domain, Vps9 (vacuolar protein sorting) domain, Sec2-domain, TRAPP (transport protein particle) complex, plus other heterodimeric complexes [reviewed in (Ishida, M et al., 2016)]. Out of these, GEFs containing Vps9 domains regulate diverse stages of endocytosis and early endosome transport. These GEFs contain ancillary domains capable of mediating interactions with proteins and lipids, also generating layers of possible regulatory steps. Given the structural complexity of GEFs containing Vps9 domains, such as those that regulate endosomal Rabs, one would hypothesize that layers of auto-regulatory steps, such as those documented for Sos, are likely found in Vps9 domain containing GEFs.

Rabex5 is the best understood member of the Vps9 domain-containing GEFs. It has a Zn finger Ubiquitin binding domain (UBD) and a motif interacting with Ubiquitin (MIU), near the N-terminus (Red in Figure 1). These domains were shown to independently bind Ubiquitin molecules and binding to Ubiquitinated cargo is thought to help Rabex5 localize to the plasma membrane or early endosomes (Mattera & Bonifacino, 2008, Penengo, Mapelli et al., 2006). A 4-helix bundle (4-HB, gold in Figure 1) is appended to the N-terminal side of the Vps9 domain and is important for stabilizing the Vps9 domain (green in Figure 1) (Delprato, Merithew et al., 2004). Together, the 4-HB and Vps9 domain make up the minimal catalytic machinery for GEF activity (Delprato et al., 2004). And finally, near the C-terminus is the Rabaptin5 binding site (RpBD, red in Figure 1) (Delprato & Lambright, 2007). Rabex5 exists in a tight complex with the Rab5 effector Rabaptin5, which regulates Rabex5 GEF activity (Delprato & Lambright, 2007, Delprato et al., 2004, Horiuchi, Lippe et al., 1997, Lippe, Horiuchi et al., 2001).

Early studies of catalysis led to the proposal that Rabex5 is in an inactive state where its C-terminus hinders Rab5 binding and, thus, auto-inhibits its GEF activity (Delprato et al., 2004). Rabaptin5 binding to the C-terminus was suggested to cause a structural rearrangement such that the Rab5 binding to Rabex5 and subsequent catalysis can proceed (Delprato & Lambright, 2007, Stenmark, Vitale et al., 1995, Zhu, Zhai et al., 2004). However, these studies utilized truncated constructs of Rabex5 and Rabaptin5. In addition, Rabex5 forms a relatively stable complex with Rabaptin5 (REF Horiuchi), raising the question of whether this allosteric mechanism is the key modulator of the GEF activity. Given its complex multi-domain organization, we reasoned that studying the full-length form of Rabex5 and its association with full-length Rabaptin5 was necessary to give a clearer picture of the auto-regulatory events. High resolution structural

techniques such as x-ray crystallography, have proven difficult for full-length Rabex5 due to localized dynamics and stability problems (Blumer, Rey et al., 2013, Delprato & Lambright, 2007, Delprato et al., 2004, Zhang, Zhang et al., 2014). One approach that can provide structural and mechanistic information is hydrogen deuterium exchange mass spectrometry (HDX-MS), because it provides structural information for highly dynamic proteins not amenable to crystallography.

Here, we generated full-length constructs of Rabex5 and Rabaptin5 and applied a combination of structural modelling, HDX-MS, mutagenesis and nucleotide exchange reactions to gain new insights into long-range allosteric interactions. Our results led us to propose a novel allosteric mechanism for regulating the nucleotide exchange catalytic process.

Results

A Compact Structure of Apo Rabex5 Revealed by XL-MS Integrative Modeling

We expressed and purified full-length Rabex5 and Rabaptin5 to study their interactions and regulation of GEF activity. Utilizing a structural proteomics approach, we used integrative modeling techniques to combine chemical crosslinking mass spectrometry (XL-MS) and available x-ray crystallographic structures to generate a structural model of full-length Rabex5 (Figure 1). As a starting point in our modeling process, we used available PDB coordinates for the UBD (blue in Figure 1), 4-HB (green), Vps9 domain (gold) and the C-terminal RpBD (red) as rigid body units for the modeling (see Methods). Additionally, we employed beads to model flexible linker regions with no crystallography data. We ran coarse-grained docking simulations to exhaustively sample the spatial configurations of rigid domains and interconnecting linkers which best satisfied MS/XL-derived spatial restraints (see Methods).

Mapping of XL-derived spatial restraints on available crystal structures immediately suggested that the Rabex5 structure in its Apo state better accommodates input XLs, primarily due to a different conformation of RpBD and of 4-HB domains. The observed conformational differences in relative positioning between the 4-HB and the Vps9 domain in Rabex5 structures (Delprato & Lambright, 2007, Delprato et al., 2004, Zhang et al., 2014), prompted us to run additional simulations allowing for rotation between the two domains forming the catalytic core. Indeed, treating the 4-HB and Vps9 domains as independent rigid bodies better satisfied XL-MS data, than if kept as a single, stably folded unit (Table S1). This suggests that there is movement and possibly rotation of the 4-HB with respect to the Vps9 domain in solution. Next, we ran additional independent simulations additionally allowing internal flexibility of the RpBD and UBD with respect to the rest of the protein. Cluster analysis on the top scoring models identified the three best representative conformers for each simulation condition and allowed us to estimate the predicted conformations that best satisfied XL-MS restraints (Table S1). Notably, the models in best agreement with the XL-MS data (99% of cross-links satisfied) are generated from trajectories allowing flexibility between the 4-HB and Vps9 domain, as well as between the RpBD and the rest of the protein.

Dissecting Rabex5 Allosteric Regulation Through HDX-MS

Given the complexity of auto-regulation for other GEFs, we sought to probe the impact of different domains of Rabex5 on the global structure of this protein, as well as its nucleotide exchange activity toward Rab5. A series of domain deletion mutants were created (Figure 2). The C-terminus of Rabex5 contains the Rabaptin5 binding domain (RpBD) (Stenmark et al., 1995, Zhu et al., 2004) and HDX-MS data isolates its start site to Gly407 (Figure S3). Deletion of that region (Gly407-Gly492) yielded the RabexΔRpBD mutant. Rabex5 contains two separate Ubiquitin binding domains (UBDs) as delineated by previous crystallography experiments (Penengo et al., 2006). For simplicity, the Zn-finger and MIU UBDs were treated as a single UBD unit. Removal of that region created the mutant, RabexΔUBD. The linker region connecting the UBDs to the 4-HB is dynamic and less well studied than the rest of the protein, so multiple deletions were created based on exploratory HDX-MS results but only one was selected for use, RabexΔ82-117 (termed RabexΔLinker). Deletion of a larger fragment (Thr82-Gln131) produced a protein which was slightly destabilized as shown by deuterium uptake and was deemed unsuitable for further use (data not shown). Finally, the RabexCAT construct was created by deleting the UBDs, the Linker, and the RpBD.

We next characterized our domain deletion mutants, by determining their nucleotide exchange activity and probing their structural alterations using HDX-MS (Figures 3 and 4, respectively). It was shown previously that Rabaptin5 binding enhanced the catalytic efficiency of Rabex5, a key finding in generating the current understanding of Rabex5 auto-regulation (Delprato & Lambright, 2007, Delprato et al., 2004). Consistent with precedent, the full-length Rabaptin5 protein showed a rate enhancement upon binding for WT Rabex5 and the Rabex5 mutants tested (Delprato & Lambright, 2007, Delprato et al., 2004, Zhang et al., 2014)(Figure S2). Full-length Rabex5, along with some of the mutant proteins, were somewhat unstable and difficult to express and purify in the absence of Rabaptin5. Thus, we compared Rabex5 domain deletion mutants only in complex with full-length Rabaptin5 (with the exception of RabexΔRpBD, which is unable to bind Rabaptin5).

It was previously suggested that the C-terminus of Rabex5 is folded over the Vps9 domain blocking the Rab5 binding site to produce auto-inhibition of nucleotide exchange activity (Delprato & Lambright, 2007, Delprato et al., 2004, Zhang et al., 2014). However, the XL-MS data

suggests otherwise. Lys433, which is located near the C-terminus within the Rabaptin5 binding domain, formed numerous cross-links with the rest of the protein. The majority of the connections were made with either the Linker or 4-HB (Figure 1). Cross-links were also made with Lys234, Lys241, and Lys304, which are adjacent to the Rab5 binding site within the Vps9 domain. However, these residues were also found to be cross-linked with Lys413, also near the C-terminus, suggesting substantial flexibility in the connectivity between the Vps9 domain and the C-terminus in the Rabex5 apo structure. Thus, our XL-MS data suggest that in apo Rabex5, the C-terminus makes contacts mainly with amino acid residues within the Linker and 4-HB. Interestingly, the Rab5 binding site within the Vps9 domain was largely free of intra-domain cross-links, which suggests that it is mainly solvent accessible rather than occluded by any other part of the protein.

To select the best structural model, we pseudo-colored the most promising structural models using the deuterium uptake of WT-Rabex5 alone and in complex with Rabaptin5. The model in best agreement with these data was generated from 4n3z with maximum flexibility. This model will be used throughout the manuscript. Figure S4 shows the deuterium uptake after 10s for apo Rabex5 and Figure 4A shows the results of Rabaptin5 binding. Two important regions of the protein with helical propensity, the MIU and RpBD are shown as stable helices even though the HDX-MS data suggests they are largely flexible in the apo state, because illustrating them as helices makes them much easier to visualize. Upon binding Rabaptin5, one sees dramatic protection of Gly407-Glu460, as expected from the formation of a dimeric coiled-coil between the two proteins. There is also mild protection extending from Asn335-Leu406, the C-terminal part of the Vps9 domain, including part of the Rab5 binding site. Again, our results are inconsistent with the hypothesis that the C-terminus of Rabex5 is folded over the Vps9 domain (Delprato & Lambright, 2007, Delprato et al., 2004, Zhang et al., 2014). Firstly, Gly407-Gly492 is highly dynamic with ~100% deuterium uptake in 10s, (Figure S4) and thus unstructured prior to binding Rabaptin5. If the C-terminus was in contact with the Vps9 domain, it should retain some structure and have considerably less than 100% deuterium uptake in 10s. Secondly, if the C-terminus were folded over the Vps9 domain, physically protecting it from solvent, one would expect enhanced deuterium exchange in the Vps9 domain upon release of the C-terminus:Vps9 domain contacts. One sees the opposite, or a protection of Asn335-Leu406 as mentioned above (Figure 4A). Also, our final structural model, which is in agreement with 99% of the XL-MS data,

shows the RpBD some distance away from the Rab5 binding site. Thus, the structural alterations in Rabex5 upon binding to Rabaptin5 are incompatible with breaking interactions between the C-terminus and the Vps9 domain.

Unexpectedly, we found protection in the Zn-finger UBD, extending Leu18-Cys38, coupled with a very mild destabilization of the MIU UBD (Trp39-Asp54), suggesting that the binding of Rabaptin5 serves to alter Ubiquitin binding by Rabex5. Another unexpected finding is enhanced exchange by the Linker residues Phe83-Glu120 upon binding Rabaptin5. Given the positioning of the Linker in a key location adjacent to the UBDs, 4-HB, Vps9 domain, and C-terminal RpBD (Figure 1), one can see how the binding of Rabaptin5 by the C-terminus could allow the Linker to move, causing the enhanced deuterium exchange as well as the aforementioned structural alterations in the UBDs and Vps9 domain. Thus, the Linker is in a key position for modulating Rabex5 structure.

Next, we compared the deuterium uptake of full-length Rabex5 with RabexΔRpBD, (Figure 4B). The results are virtually identical to those induced by Rabaptin5 binding to full-length Rabex5, suggesting that the allosteric structural alterations in Rabex5 are caused primarily by breaking contacts made between the RpBD and the Linker, causing the enhanced deuterium uptake in the Linker upon binding Rabaptin5 or deletion of the RpBD in Rabex5 (Figure 4A, B).

Linking Allosteric Regulation with Kinetics of GEF Activity

To further dissect potential interactions between domains, we examined the RabexΔUBD mutant, which had a ~2-fold increase in nucleotide exchange activity (Figure 3), suggesting that the UBDs play a key role in the auto-regulation of Rabex5 GEF activity. Removal of the UBDs also created a destabilization of Ile339-Phe382, which encompasses part of the Rab5 binding site within the Vps9 domain (Figure 4C). This suggests that the presence of the UBDs stabilizes the Vps9 domain and auto-inhibits nucleotide exchange activity. Our current structural model of Rabex5 (Figure 1) places the Zn-finger UBD on the opposite side of the protein relative to the Rab5 binding site, so a *direct* interaction is not feasible. If the UBDs serve an auto-regulatory role for Rabex5, one would expect that Ubiquitin binding would modulate nucleotide exchange activity in Rabex5. To test this hypothesis, we monitored the effect of Ubiquitin on the nucleotide exchange activity of Rabex5. The EGF receptor is Ubiquitylated via a Lys63 linkage during

endocytic processing (Haglund & Dikic, 2012). Thus, we hypothesized that Lys63 linked tetra-Ubiquitin might play a role in modulating Rabex5 localization and Rab5 activation. We found that Lys63 tetra-Ubiquitin stimulated nucleotide exchange in a concentration-dependent manner (Figure 5). This suggests that Ubiquitin binding could not only localize Rabex5 to an endosome containing Ubiquitylated cargo, but also enhance Rab5 GEF activity at that location, thus activating Rab5 in a cargo-specific manner.

Removal of 82-117 in RabexΔLinker caused a ~50% loss in nucleotide exchange activity, suggesting an unexpected role for this region in modulating catalysis (Figure 3). This is combined with an increase in deuterium uptake over the entire Rabaptin5 binding site (Gly407-Glu460), with the most dramatic effect localized to Met422-Glu431 (Figure 4D). Given that the structural alterations are limited to the RpBD, one can exclude global misfolding of this mutant leading to the decreased enzymatic activity. This suggests an important and hitherto undocumented role by the Linker in modulating both nucleotide exchange and interaction with Rabaptin5. Removal of the Linker region in Rabex5 resulted in destabilization of the RpBD, but caused no detectable difference in complex formation, dimerization of the complex, or deuterium uptake in Rabaptin5 (data not shown). The cross-linking data illustrate the central position the Linker holds within Rabex5. The Linker forms numerous cross-links with the MIU, 4-HB, Vps9 domain, and the C-terminal RbBD (Figure 1). Together these cross-links account for just over 41% of the total, while the Linker accounts for less than 5% of Rabex5, suggesting that it holds a key position in Rabex5 for mediating inter-domain communication and auto-regulation.

Much of the current understanding of the Rabex5 catalytic core structure and nucleotide exchange was derived from a construct containing Rabex132-394, because it was sufficient for catalysis while being amenable to crystallization (Delprato & Lambright, 2007, Delprato et al., 2004, Zhang et al., 2014). We expressed and purified this protein and characterized it by HDX-MS. The results show this construct to be substantially destabilized through the entire 4-HB and Vps9 domain compared with the full-length Rabex5 (Figure S1a). We generated a construct similar to Rabex132-394, but with slightly different start and end points such that it aligned better with our mutants. The resulting protein, RabexCAT, was also dramatically destabilized compared with WT Rabex5 protein (Figure S1b). Its nucleotide exchange activity was roughly 2-fold higher than WT

Rabex5:Rabaptin5 complex (Figure 3), but interpretation of results is clouded by the widespread instability of the protein.

To delve more deeply into the process of nucleotide exchange, we monitored the deuterium uptake of Rabex5 and Rabaptin5 during the GTPγS loading process. To ensure formation of a ternary Rabex5:Rabaptin5:Rab5 complex, Rabex5:Rabaptin5 was pre-incubated with a 5-fold molar excess of GDP-bound Rab5. The mixture was subsequently incubated ± GTPγS in deuterated buffer for 60, 300 or 900s. The Zn-finger UBD showed decreased deuterium uptake and thus was stabilized during the nucleotide exchange process (Figure 6). Stabilization of the UBD is likely due to the release of Rab5 after nucleotide exchange, as the binding of inactive Rab5 to the Rabex5:Rabaptin5 complex causes destabilization of the Zn-finger UBD (data not shown). There is also mild destabilization of portions of the 4-HB and Vps9 domain, suggesting that nucleotide exchange is coupled with backbone motions within parts of the 4-HB and Vps9 domain. This helps explain why enhanced flexibility in parts of the catalytic core is correlated with increased nucleotide exchange, as was shown in the domain deletion mutants, RabexΔUBD (Figure 4c), RabexΔ82-132 (data not shown), Rabex132-394, (Figure S1), and our RabexCAT (Figure S1). Each of these constructs showed enhanced backbone dynamics within the catalytic core and enhanced nucleotide exchange activity compared with full-length Rabex5. Unexpectedly, during the first minute of GTPγS exchange reaction, peptides from the Linker region Glu87-Glu120 in Rabex5 disappeared followed by reappearance after 300s (Figure 7B, 7D). The recovery of these peptides continued in the 900s time point (data not shown). Similar trends were seen in multiple overlapping peptides in Rabaptin5 (Leu316-Glu342) and for both proteins, only in the presence of GTPγS, suggesting this is caused by the nucleotide exchange process rather than a technical artifact. These data further support the idea that part of the Rabex5 Linker, specifically Glu87-Glu120 plays an important role in modulating Rabex5 structure as well as nucleotide exchange. Taken together, these data give us new insights and previously unrecognized roles for the Zn-finger UBD as well as the linker in the auto-regulation of Rabex5.

Discussion

It has long been known that Rabex5 GEF is stimulated by Rabaptin5 and binds Ubiquitin (Blumer et al., 2013, Delprato & Lambright, 2007, Horiuchi et al., 1997, Lippe, Miaczynska et al., 2001, Mattera & Bonifacino, 2008). In this work we aimed at gaining a clearer picture of how Rabex5 is regulated by studying full-length Rabex5 and Rabaptin5, retaining all relevant binding sites and three-dimensional structure, using a structural proteomics approach including XL-MS and HDX-MS. Comparisons between full-length proteins and domain deletion mutants yielded new insights that were not previously revealed with truncated proteins. We could provide evidence of long-range interactions between the RpBD and the Linker, which by modulating the structure of the Vps9 domain, regulate its nucleotide exchange activity. Our results may have implications for the allosteric activation of Rab GEFs as well as GEFs for small GTPases in general.

We propose a novel model to explain how allosteric modulation of Rabex5 structure regulates endosomal Rab5 activation during cargo transport. Rabaptin5 is complexed to Rabex5 and this interaction is required to confer stability and allosteric regulation on Rabex5 catalytic GEF activity. However, the structural changes upon complex formation are incompatible with the previously proposed interactions between the C-terminus and the Vps9 domain of Rabex5. Instead, from our analyses emerged a more important role of the UBD in modulating such activity. It was previously proposed that Ubiquitin binding serves to localize Rabex5 on the endosomal membrane (Blumer et al., 2013, Mattera & Bonifacino, 2008, Penengo et al., 2006). Our results indicate that binding of Ubiquitin to the UBD of Rabex5 goes beyond mere recruitment as it also enhances nucleotide exchange activity. This implies that endocytosis of Ubiquitinated cargo, would supply binding sites for Rabex5 or the Rabex5:Rabaptin5 complex, localizing and enhancing Rab5 activation on early endosomes. Being a Rab5 effector, Rabaptin5 can also bind active Rab5, stabilizing it on the endosomal membrane (Horiuchi et al., 1997, Stenmark et al., 1995). This serves to create a positive feedback loop (Horiuchi et al., 1997), whereby stimulation of Rab5 activity would enhance early endosome fusion, regulating the life-time of endocytosed receptors in early endosomes (Villasenor, Nonaka et al., 2015). This is consistent with the long observed increase in early endosome fusion following internalization of EGFR (Benveniste, Schlessinger et al., 1989, Roberts, Barbieri et al., 2000, Sorkin, McClure et al., 2000) in addition to

micropinocytosis (Argenzio, Bange et al., 2011, Balaji, Mooser et al., 2012, Horiuchi et al., 1997, Penengo et al., 2006, Sonnichsen, De Renzis et al., 2000).

The availability of full-length proteins was of fundamental importance to obtain insights into Rabex5 structure and regulation. For example, in the full-length proteins, the interaction site between Rabex5 and Rabaptin5 was localized to Gly407-Glu460 in Rabex5 and Met563-Leu658 in Rabaptin5, with the core of the interaction site and most dramatic protection localized to Val600-Leu633. This differs slightly from the structure portrayed by PDB:4q9u, which shows interaction between Pro392-Ile453 in Rabex5 and Phe584-Arg635 in Rabaptin5 (Zhang et al., 2014). The constructs used to generate PDB:4Q9U were truncated to enhance crystallization. While their construct, Rabaptin5 (552-642) binds Rabex5, the exact region making contacts differs from that observed here using full-length construct. The most dramatic difference between our results and those of PDB:4q9u, 4n3y, and 4n3z are that they display an arrangement of Rabaptin5:Rabex5 (2:1) (Zhang et al., 2014). Our size exclusion coupled with static light scattering results clearly show a 1:1 arrangement (data not shown). Since the structures reported in Zhang *et al.* were generated with a Rabaptin5 peptide covering 552-642, one can hypothesize that the differences are caused by a non-physiological pairing of the coiled coil with such a limited portion of Rabaptin5.

One other potentially important difference between our results and those derived from crystallography is the relative positioning of the 4-HB with respect to the Vps9 domain. The relative positions of these domains in 4q9u differ slightly from that of 4n3z. Our modeling simulations generated structures in better agreement with XL-MS data when flexibility was allowed between the 4-HB and Vps9 domain. This suggests that flexibility or possibly rotation between the domains occurs in solution. Is this rotation merely the normal “breathing” which occurs in proteins, or is it a relevant part of the nucleotide exchange mechanism? The HDX-MS results obtained during catalysis by the Rabex5:Rabaptin5 complex showed enhanced deuterium exchange occurring in the catalytic core of Rabex5 (Figure 6). Specifically, parts of both 4-HB and Vps9 were affected, leaving us to postulate that if increased backbone dynamics within the catalytic core occur during nucleotide exchange, anything restricting mobility in these regions could decrease GEF activity and, conversely, anything enhancing mobility could increase it. The domain deletion mutants showed us that deletions which caused enhanced deuterium uptake

(enhanced mobility or flexibility) within the 4-HB and/or Vps9 domain correlated with increased nucleotide exchange activity for Rab5. This is an entirely new way of thinking about Rabex5 auto-regulation.

The role of UBDs in the auto-regulation of Rabex5 was unexpected. Our results show that deletion of the UBDs causes a 2-fold increase in nucleotide exchange as well as enhanced deuterium uptake in a portion of the Rab5 binding site. The HDX-MS results for the C-terminal deletion mutant of Rabex5, RabexΔRpBD or the binding of full-length Rabex5 to Rabaptin5 via the C-terminus both alter the structure of the UBDs. This long-range allosteric regulation as well as enhancement of Rabex5 GEF activity by Ubiquitin binding has never been revealed before and suggests a major role for Ubiquitin in regulating Rabex5. A study of the evolution of the Vps9 domain showed 3 independent instances of acquisition of structurally diverse UBDs: the ZnF in mammalian Rabex5, the CUE domain in yeast, and a UBD in the amebozoan *Sexangularia sp.* (Herman, Ali et al., 2018). The fact that Vps9 domain containing proteins had such a strong tendency to acquire UBD through independent means suggests a critical role for UBDs in regulating Vps9 activity.

Another previously unknown phenomenon in Rabex5 is the communication between the C-terminus and UBDs, which seems to be mediated by the Linker. This is not the first example of a Linker being more than just a flexible tether between domains within a GEF (Cherfils & Zeghouf, 2013). The release of the Linker upon binding Rabaptin5 (Figure 4A,B) suggested a critical connection between the Linker and the RpBD. Our results show an unequivocal connection between these regions since the RabexΔLinker mutant displayed enhanced deuterium uptake in the RpBDand the RabexΔRpBD mutant displayed enhanced deuterium uptake in the Linker (Figure 4C,D). Careful inspection of our molecular model of Rabex5 shows that the Linker is located in a critical position between the RpBD, 4-HB, Vps9 domain, and UBDs. Thus, one can see how moving the Linker can alter the entire protein and regulate GEF activity. Sequence alignment of Rabex5 with its two most similar Vps9 domain containing proteins, Gapex5 and Varp5, show that Ala123 and Pro124 within the Linker region are strictly conserved. Deletion of Thr82-Gln131 caused unexpected destabilization of the 4-HB, which was not present when only Thr82-Glu117 was deleted. Also, Rabex132-394 and RabexCAT were found to be substantially destabilized compared with WT Rabex5 (Figure S1). The HDX-MS results suggest that a portion of the Linker,

specifically Ile118-Gln131 stabilizes or regulates the catalytic core. Sequence conservation suggests Ala123 and Pro124 could be mediating this activity.

In summary, our results show that auto-regulation of Rabex5 GEF activity is more sophisticated than previously appreciated. Using the full-length protein, as well as domain deletion mutants, helped us reveal some of the depth of auto-regulation of Rabex5, which was missed in previous studies. Specifically, the Linker and RpBD show correlated behavior suggesting direct contact. If this interaction is modulated, allosteric structural alterations in the UBD and Vps9 domain as well as enhanced nucleotide exchange follow. Our results correlating enhanced flexibility within the catalytic core with increased nucleotide exchange activity suggest an additional means of regulating nucleotide exchange. These results reveal layers of auto-regulation not previously suggested for Rabex5 and suggests that other GEFs may also contain as yet unappreciated regulatory mechanisms.

Materials and Methods

Expression and Purification of Recombinant Proteins

The gene sequences corresponding to full-length bovine Rabex5 (1-492) and full-length human Rabaptin5 (1-862) were subcloned into 6x-His or GST-containing pOEM derived vectors for baculoviral expression. Each vector contains an HRV 3C-cleavage site to remove purification tags from the desired protein. SF+ cells growing in ESF921 media (Expression Systems) are transfected with plasmid and in-house prepared bacmid DNA. Conditioned media containing virus is harvested and used to infect SF+ cells at 1% vol/vol. Cells are harvested after 40-48 h and frozen. Human Rab5a in a pGEX-5x vector is transformed in BL21(DE3) cells. Protein expression is induced by 0.1 mM isopropyl-1-thio-b-D-galactopyranoside to the culture. Cells are harvested after 18 h at 16 degC and frozen. All cell pellets are resuspended in 40mL of Rab5 buffer (20mM tris pH 7.4, 150mM NaCl, 5mM $MgCl_2$, 0.5 mM TCEP) plus protease inhibitor cocktail (chymostatin 6 ug/mL, leupeptin 0.5 ug/mL, antipain-HCl 10ug/mL, aprotinin 2ug/mL, pepstatin 0.7 ug/mL APMSF 10ug/mL) and lysed by sonication. Lysates were clarified by centrifugation and applied to Ni-NTA resin in the presence of 20 mM imidazole or GS-4B resin for 2 h at 4 degC, followed by stringent washing. While on GS-resin, Rab5 is washed with Rab buffer containing 10 mM EDTA to remove endogenous nucleotide and returned to Rab buffer for cleavage from the resin. To generate GTPγS-Rab5, GS-bound protein is washed with Rab buffer containing 10 mM EDTA and 1 mM GTPγS and subsequently returned to Rab5 buffer for cleavage from the resin. All proteins are incubated with HRV 3C protease (Rabex5 and Rabaptin5) or Factor X_a (Rab5) overnight at 4 degC with mixing and further purified by size exclusion chromatography using S200 or Superose 6 columns. Concentrations are determined using a BCA assay (Thermo Scientific) and proteins are stored at -80 degC.

Chemical Crosslinking combined with Mass Spectrometry (XL-MS)

To provide distance constraints for modelling of Rabex5, XL-MS has been applied according to protocols recently published in (Guaitoli, Raimondi et al., 2016). Briefly, in order to obtain a cross linker to protein ratio of 12.5:1 or 25:1, NHS-ester–based chemical cross-linking was performed adding DSS H12/D12 or DSG-H6/D6 solution (both at a 12.5 mM stock solution in

DMSO) to 80 µg of purified protein in HEPES-based buffer. The reactions were carried out under constant rotation at RT for 30 min. Reaction was then quenched adding Tris·HCl (pH 7.5) solution to a final concentration of 10 mM and incubated again for another 15 min at RT under constant shaking. After quenching, protein samples were precipitated using chloroform and methanol. Proteolysis was performed, and the resulting peptide mixtures were separated by size exclusion chromatography to enrich cross-linked peptides. For mass spectrometric analysis, SpeedVac-dried SEC-Fractions were re-dissolved in 0.5% TFA and analyzed by LC-MSMS using a nano-flow HPLC system (Ultimate 3000 RSLC, Thermo-Fisher) coupled to an Orbitrap Fusion (Thermo-Fisher) tandem mass spectrometer. For identification, crosslinked peptides were separated and analyzed by a data-dependent approach acquiring CID MSMS spectra of the 10 most intense peaks (TOP 10), excluding single and double charged ions. Prior to analysis via xQuest/xProphet (V2.1.1), MSMS spectra were extracted from the RAW files using ProteoWizard/msconvert (3.0.6002). The identification of monolinks, looplinks and crosslinks was done based on the identification of DSS H12/D12 or DSG H6/D6 pairs. For xQuest/xProphet, standard parameters were used with methionine oxidation as variable modification. For DSS-D12 and DSG-D6, isotope differences of 12.075321 Da and 6.03705 Da were used, respectively. The parent ion tolerance was set to 10 ppm (MS) and the fragment ion tolerance to 0.3 Da (MSMS). Only those crosslinked peptides were considered for modelling which fulfilled the following minimal criteria: ID-score>28, deltaS<0.95, FDR<0.05. Additionally, the MSMS spectra were evaluated by manual inspection to ensure a good representation of the fragment series of both crosslinked peptides.

Structural Modelling

We generated a structural input model of full length Rabex5 in its apo state using available x-ray structures of Rabex5 (PDB ID: 4N3Z and 2C7N). In order to achieve a full-length model, we created linkers joining the N-terminal helix bound to Ubiquitin (PDB ID: 2C7N) to the 4-HB, Vps9 and C-terminal domains (PDB ID: 4N3Z) through Modeller (Sali & Blundell, 1993). A total of 100 models were generated by randomizing the amino acid Cartesian coordinates in the initial model. The twenty models with the lowest number of stereochemical constraints violations were selected and ranked according to the DOPE score (Shen & Sali, 2006) The best ten models were validated for their stereochemical quality through the Molprobity tool (Chen, Arendall et al.,

2010) available in the Phenix software package (Adams, Afonine et al., 2011) and the best scoring model was retained for further modeling steps. We also derived through the same strategy an alternative starting conformation by considering Rabaptin-bound Rabex structure (PDB ID: 4Q9U).

Determining the Rabex in the APO state with Integrative Modeling Platform (IMP)

We predicted the 3D structure of full length Rabex in its apo state by using XL/MS-derived distance restrained docking calculations through the Integrative Modeling Platform (IMP) (Russel, Lasker et al., 2012) package, release 2.9.0. We employed the Python Modeling Interface (PMI), adapting the scripted pipeline of a previously described procedure (Chen, Pellarin et al., 2016) and consisting in the following key steps: (1) gathering of data, (2) representation of domains and/or subunits and translation of the data into spatial restraints, (3) configurational sampling to produce an ensemble of models that optimally satisfies the restraints, and (4) analysis and assessment of the ensemble.

System representation

The full-length Rabex initial models were used as input structures for IMP calculations. Domains of Rabex structures were represented by beads arranged into either a rigid body or a flexible string on the basis of the available crystallographic structure. We probed as input for simulation both the apo state (PDB ID: 4N3Z), as well as the Rabaptin/Rab5 bound (PDB ID: 4Q9U) Rabex x-ray structures. We also included the structure of the Ubiquitin bound N-terminal helix (PDB ID: 2C7N). The beads representing a structured region were kept rigid with respect to one another during configurational sampling (i.e. rigid bodies). The following regions have been defined as rigid body entities: N-terminal α-helix (NtH):18-71; 4 Helical Bundle (4-HB): 133-228; Vps9: 231-368; C-terminal α-helix (CtH): 408-452. The Ubiquitin structure (residues: 1-73) was considered as a single rigid body unit together with the NtH. Protein segments without a crystallographic structure or the linkers between the rigid domains were represented by a flexible string of beads, where each bead corresponded to a single residue. For both starting configurations, we performed two simulation sets: one where the 4-HB and Vps9 domains were kept as a single rigid

body and the other where they were kept as independent rigid body (i.e. introducing flexible beads at residues 229-230).

Bayesian Scoring Function

The cross-linking data were encoded into a Bayesian scoring function that restrained the distances spanned by the cross-linked residues (Erzberger, Stengel et al., 2014). The Bayesian approach estimates the probability of a model, given information available about the system, including both prior knowledge and newly acquired experimental data (Erzberger et al., 2014, Rieping, Habeck et al., 2005). Briefly, using Bayes' theorem, we estimate the posterior probability p(M D,I), given data D and prior knowledge I, as p(M D, I) $\propto$ p(D M, I)p(M, I), where the likelihood function p(D M,I) is the probability of observing data D, given I and M, and the prior is the probability of model M, given I. To define the likelihood function, one needs a forward model that predicts the data point (i.e. the presence of a cross-link between two given residues) given any model M and a noise model that specifies the distribution of the deviation between the observed and predicted data points. To account for the presence of noisy cross-links, we parameterized the likelihood with a set of variables $\{\psi\}$ defined as the uncertainties of observing the cross-links in a given model (Erzberger et al., 2014, Robinson, Trnka et al., 2015). A distance threshold of 20 Å was employed to model DSSO cross-linkers.

Sampling Model Configurations

Structural models were obtained by Replica Exchange Gibbs sampling, based on Metropolis Monte Carlo sampling (Rieping et al., 2005). This sampling was used to generate configurations of the system as well as values for the uncertainty parameters. The Monte Carlo moves included random translation and rotation of rigid bodies (4 Å and 0.03 rad, maximum, respectively), random translation of individual beads in the flexible segments (5 Å maximum), and a Gaussian perturbation of the uncertainty parameters. A total of 500,000 models per system were generated, starting from 100 random initial configurations and sampling with temperatures ranging between 1.0 and 2.5. We divided this set of models into two ensembles of the same size to confirm sampling convergence (data not shown).

Analysis of the Model Ensemble

The 200 best scoring models (i.e. solutions) for each docking run were clustered to yield the most representative conformations. For each ensemble, the solutions were grouped by k-means clustering on the basis of the r.m.s. deviation of the domains after the superposition of the Vps9 domain (Figure 1). The precision of a cluster was calculated as the average r.m.s. deviation with respect to the cluster center (i.e. the solution with the lowest r.m.s. deviation with respect to the others).

For each cluster, we calculated the number of satisfied MS/XL by measuring the number of Cα pairs, corresponding to cross-linked lysines, whose distance was shorter than 34 Å. We recorded the fraction of satisfied cross-links, given by the number of satisfied XLs over the total, for all the cluster members. We finally reported the fraction of satisfied XLs for the best scoring solution, as well as the maximum fraction obtained for a single cluster conformer and the aggregate fraction obtained by considering all the cluster members together.

For visualization purposes, we generated all atoms models by starting from the Cα traces generated from IMP and using the *automodel()* function from Modeller (Sali & Blundell, 1993).

Hydrogen Deuterium Exchange Mass Spectrometry

HDX-MS was performed essentially as previously described (He, Bai et al., 2015, Mayne, Kan et al., 2011, Walters, Ricciuti et al., 2012). Proteins (1 uM) are diluted 6:4 with 8M urea, 1% trifluoroacetic acid, passed over an immobilized pepsin column (2.1 mm x 30 mm, ThermoFisher Scientific) in 0.1% trifluoroacetic acid at 15 degC. Peptides are captured on a reversed-phase C8 cartridge, desalted and separated by a Zorbax 300SB-C18 column (Agilent) at 1 degC using a 5-40% acetonitrile gradient containing 0.1% formic acid over 10 min and electrosprayed directly into an Orbitrap mass spectrometer (LTQ-Orbitrap XL, ThermoFisher Scientific) with a T-piece split flow setup (1:400). Data were collected in profile mode with source parameters: spray voltage 3.4kV, capillary voltage 40V, tube lens 170V, capillary temperature 170degC. MS/MS CID fragment ions were detected in centroid mode with an AGC target value of 10^4. CID fragmentation was 35% normalized collision energy (NCE) for 30 ms at Q of 0.25. HCD fragmentation NCE was 35eV. Peptides were identified using Mascot (Matrix Science) and manually verified to remove ambiguous peptides. For measurement of deuterium uptake, 10uM protein is diluted 1:9 in Rab5

buffer prepared with deuterated solvent. Samples were incubated for varying times at 22 deg C followed by the aforementioned digestion, desalting, separation and mass spectrometry steps. The intensity weighted average m/z value of a peptide's isotopic envelope is compared plus and minus deuteration using the HDX workbench software platform. Individual peptides are verified by manual inspection. Data are visualized using Pymol. Deuterium uptake is normalized for back-exchange when necessary by comparing deuterium uptake to a sample incubated in 6M urea in deuterated buffer for 12-18h at room temperature and processed as indicated above.

Nucleotide Exchange Kinetics

Nucleotide exchange kinetics were measured by monitoring the release of the mant-GDP nucleotide analog, 2′-(3′)-bis-O-(N-methylanthraniloyl)-GDP (Jena Biosciences). Rab5 was loaded with mant-GDP in Rab5 buffer + 10mM EDTA and 5-fold excess mant-GDP. Rab5(mant-GDP) was separated from unbound nucleotide by size exclusion chromatography using Rab5 buffer. Samples were excited at 355 nm and the emission monitored at 448 nm. Reactants were mixed in 20mM tris (pH 8), 150mM NaCl, 0.5mM $MgCl_2$. Exchange reactions were initiated by addition of 200µM GTP. Data were collected using a Spark microplate spectrophotometer (Tecan). Observed pseudo-first order rate constants (k_{obs}) were calculated in Prism using the one phase decay non-linear fit. The catalytic efficiency, k_{cat}/K_m, was obtained by subtracting the intrinsic rate (k_{intr}) of GDP release and dividing by the concentration of Rabex5.

Acknowledgements

We warmly thank Ramona Schäfer and the Core Facility for Bioanalytics at the University of Tübingen for technical assistance as well as the Mass Spectrometry Facility at Max Planck Institute of Molecular Cell Biology and Genetics for access to their facilities.

Author Contributions

JL coordinated the study, prepared all proteins, designed, performed and analyzed the HDX-MS experiments, and wrote the manuscript. AC helped design and create Rabex5 mutants and contributed to writing the manuscript. GG performed the XL-MS experiments, analyzed the data, and contributed to writing the manuscript. VA, MH, and FR contributed to creation of the structural models and writing the manuscript. MU and CJG supervised the XL-MS experiments. MG contributed to the HDX-MS experiments. AL supervised creation of the structural models. MZ aided in experimental design and contributed to writing the manuscript.

Conflict of Interest

The authors declare that they have no conflicts of interest.

Figure Legends

Figure 1: Rabex5 XL-MS Data and Structural Model

A: The XL-MS data is shown for apo Rabex5 and illustrated in Xwalk (Kahraman, Malmstrom et al., 2011). Ubiquitin binding domains (red), Linker (teal), 4-helical bundle (gold), Vps9 domain (green), and Rabpatin5 binding domain (blue). **B**: A structural model of apo Rabex5 is pseudo-colored as illustrated above. This model is one of the possible arrangements and was chosen because it was in best agreement with the XL-MS and HDX-MS data.

Figure 2: Domain Deletion Mutants

A series of domain deletion mutants were created as indicated. Rabex5 amino acid numbering is shown for comparison.

Figure 3: Rabex5 Nucleotide Exchange Kinetics

Nucleotide exchange kinetics are shown for wild-type Rabex5:Rabaptin5 complex as well as the domain deletion mutants, all in complex with full-length Rabaptin5 (where applicable). **A**: A single

replicate data trace is shown. WT complex (blue diamonds), RabexΔRpBD (orange dashes), RabexΔUBD complex (green triangles), RabexΔLinker (purple squares), RabexCAT (blue squares). All enzymes were used at 0.5μM with the exception of RabexCAT, which was used at 0.25μM. **B**: A compilation of nucleotide exchange kinetics data is shown. Averages were calculated from 3 individual experiments containing 3 replicates.

Figure 4: HDX-MS Data

This figure shows differential uptake of deuterium. In each case, the coloring scheme is as follows: none statistically different uptake (grey), regions missing peptide coverage(white), regions deleted in mutants (magenta), regions protected from exchange (cool colors, as shown in the figure), and regions showing enhanced exchange (warm colors, as shown in the figure). **A:** WT Rabex5 vs Rabex5:Rabaptin5 Complex, **B**: WT Rabex5 vs RabexΔRpBD, **C**: WT Rabex5:Rabaptin5 Complex vs RabexΔUBD:Rabaptin5 Complex, **D**: WT Rabex5:Rabaptin5 Complex vs RabexΔLinker:Rabaptin5 Complex.

Figure 5: Effects of TetraUb on Nucleotide Exchange

Nucleotide exchange kinetics in the absence or presence of Lys63 linked tetraUbiquitin. Panel **A** shows an example data trace for WT Rabex5:Rabaptin5 complex alone (dark blue) and plus tetraUb (light blue). Panel **B** shows an example data trace for RabexΔUb:Rabaptin5 complex alone (dark rust) and plus tetraUb (light rust). Panel **C** shows the average of 2 experiments each containing 3 replicates for WT Rabex5:Rabaptin5 complex (blue squares) and RabexΔUb:Rabaptin5 complex (rust diamonds) with varying concentrations of tetraUb.

Figure 6: HDX-MS Results During Nucleotide Exchange

The differential uptake of deuterium occurring during the nucleotide exchange reaction are illustrated using our structural model. In each case, the coloring scheme is as follows: no statistically different uptake (grey), regions missing peptide coverage(white), regions protected from exchange (pale green), and regions showing enhanced exchange (yellow).

Figure 7: Peptide Profiles During Nucleotide Exchange

Total ion current and centroid spectra for a peptide corresponding to Rabex5 (83-120) in the presence (B and D) or absence of GTPγS (A and C) after 60s (A and B) or 300s (C and D) of deuterium uptake. Note the disappearance of signal at 60s upon addition of GTPγS and partial recovery at 300s.

Supplementary Table S1:

The results of the last round of modeling are shown comparing the top scoring clusters from each condition with the XL-MS data.

Supplementary Figure S1: HDX-MS Data

This figure shows differential uptake of deuterium for **A**: WT Rabex5 vs Rabex132-394 and **B**: Rabex 132-394 vs RabexCAT, displayed on pdb:1txu. In each case, the coloring scheme is as follows: none statistically different uptake (grey), regions missing peptide coverage(white), and regions showing enhanced exchange (yellow).

Supplementary Figure S2: Nucleotide Exchange Kinetics

Nucleotide exchange kinetics are shown for wild-type Rabex5:Rabaptin5 complex as well as the domain deletion mutants, all in complex with full-length Rabaptin5 (where applicable).

Supplementary Figure S3: Deuterium Uptake in Rabex5

The results of 10s deuterium uptake are shown for WT apo Rabex5, using the indicated color scheme. The region in white has no peptide coverage.

Supplementary Figure S4: Raw HDX-MS Data

The results of individual experiments used to pseudocolor the models. In each case there is a title showing where the data was used within the manuscript.

References

Adams PD, Afonine PV, Bunkoczi G, Chen VB, Echols N, Headd JJ, Hung LW, Jain S, Kapral GJ, Grosse Kunstleve RW, McCoy AJ, Moriarty NW, Oeffner RD, Read RJ, Richardson DC, Richardson JS, Terwilliger TC, Zwart PH (2011) The Phenix software for automated determination of macromolecular structures. Methods 55: 94-106

Argenzio E, Bange T, Oldrini B, Bianchi F, Peesari R, Mari S, Di Fiore PP, Mann M, Polo S (2011) Proteomic snapshot of the EGF-induced ubiquitin network. Mol Syst Biol 7: 462

Balaji K, Mooser C, Janson CM, Bliss JM, Hojjat H, Colicelli J (2012) RIN1 orchestrates the activation of RAB5 GTPases and ABL tyrosine kinases to determine the fate of EGFR. J Cell Sci 125: 5887-96

Benveniste M, Schlessinger J, Kam Z (1989) Characterization of internalization and endosome formation of epidermal growth factor in transfected NIH-3T3 cells by computerized image-intensified three-dimensional fluorescence microscopy. J Cell Biol 109: 2105-15

Blumer J, Rey J, Dehmelt L, Mazel T, Wu YW, Bastiaens P, Goody RS, Itzen A (2013) RabGEFs are a major determinant for specific Rab membrane targeting. J Cell Biol 200: 287-300

Bos JL, Rehmann H, Wittinghofer A (2007) GEFs and GAPs: critical elements in the control of small G proteins. Cell 129: 865-77

Chen VB, Arendall WB, 3rd, Headd JJ, Keedy DA, Immormino RM, Kapral GJ, Murray LW, Richardson JS, Richardson DC (2010) MolProbity: all-atom structure validation for macromolecular crystallography. Acta Crystallogr D Biol Crystallogr 66: 12-21

Chen ZA, Pellarin R, Fischer L, Sali A, Nilges M, Barlow PN, Rappsilber J (2016) Structure of Complement C3(H2O) Revealed By Quantitative Cross-Linking/Mass Spectrometry And Modeling. Mol Cell Proteomics 15: 2730-43

Cherfils J, Zeghouf M (2011) Chronicles of the GTPase switch. Nat Chem Biol 7: 493-5

Cherfils J, Zeghouf M (2013) Regulation of small GTPases by GEFs, GAPs, and GDIs. Physiol Rev 93: 269-309

Delprato A, Lambright DG (2007) Structural basis for Rab GTPase activation by VPS9 domain exchange factors. Nat Struct Mol Biol 14: 406-12

Delprato A, Merithew E, Lambright DG (2004) Structure, exchange determinants, and family-wide rab specificity of the tandem helical bundle and Vps9 domains of Rabex-5. Cell 118: 607-17

Erzberger JP, Stengel F, Pellarin R, Zhang S, Schaefer T, Aylett CHS, Cimermancic P, Boehringer D, Sali A, Aebersold R, Ban N (2014) Molecular architecture of the 40SeIF1eIF3 translation initiation complex. Cell 158: 1123-1135

Guaitoli G, Raimondi F, Gilsbach BK, Gomez-Llorente Y, Deyaert E, Renzi F, Li X, Schaffner A, Jagtap PK, Boldt K, von Zweydorf F, Gotthardt K, Lorimer DD, Yue Z, Burgin A, Janjic N, Sattler M, Versees W, Ueffing M, Ubarretxena-Belandia I et al. (2016) Structural model of the dimeric Parkinson's protein LRRK2 reveals a compact architecture involving distant interdomain contacts. Proc Natl Acad Sci U S A 113: E4357-66

Haglund K, Dikic I (2012) The role of ubiquitylation in receptor endocytosis and endosomal sorting. J Cell Sci 125: 265-75

Hall BE, Yang SS, Bar-Sagi D (2002) Autoinhibition of Sos by intramolecular interactions. Front Biosci 7: d288-94

He W, Bai G, Zhou H, Wei N, White NM, Lauer J, Liu H, Shi Y, Dumitru CD, Lettieri K, Shubayev V, Jordanova A, Guergueltcheva V, Griffin PR, Burgess RW, Pfaff SL, Yang XL (2015) CMT2D neuropathy is linked to the neomorphic binding activity of glycyl-tRNA synthetase. Nature 526: 710-4

Herman EK, Ali M, Field MC, Dacks JB (2018) Regulation of early endosomes across eukaryotes: Evolution and functional homology of Vps9 proteins. Traffic 19: 546-563

Horiuchi H, Lippe R, McBride HM, Rubino M, Woodman P, Stenmark H, Rybin V, Wilm M, Ashman K, Mann M, Zerial M (1997) A novel Rab5 GDP/GTP exchange factor complexed to Rabaptin-5 links nucleotide exchange to effector recruitment and function. Cell 90: 1149-59

Ishida M, M EO, Fukuda M (2016) Multiple Types of Guanine Nucleotide Exchange Factors (GEFs) for Rab Small GTPases. Cell Struct Funct 41: 61-79

Kahraman A, Malmstrom L, Aebersold R (2011) Xwalk: computing and visualizing distances in cross-linking experiments. Bioinformatics 27: 2163-4

Lee YK, Low-Nam ST, Chung JK, Hansen SD, Lam HYM, Alvarez S, Groves JT (2017) Mechanism of SOS PR-domain autoinhibition revealed by single-molecule assays on native protein from lysate. Nat Commun 8: 15061

Lippe R, Horiuchi H, Runge A, Zerial M (2001) Expression, purification, and characterization of Rab5 effector complex, rabaptin-5/rabex-5. Methods Enzymol 329: 132-45

Lippe R, Miaczynska M, Rybin V, Runge A, Zerial M (2001) Functional synergy between Rab5 effector Rabaptin-5 and exchange factor Rabex-5 when physically associated in a complex. Mol Biol Cell 12: 2219-28

Mattera R, Bonifacino JS (2008) Ubiquitin binding and conjugation regulate the recruitment of Rabex-5 to early endosomes. EMBO J 27: 2484-94

Mayne L, Kan ZY, Chetty PS, Ricciuti A, Walters BT, Englander SW (2011) Many overlapping peptides for protein hydrogen exchange experiments by the fragment separation-mass spectrometry method. J Am Soc Mass Spectrom 22: 1898-905

Penengo L, Mapelli M, Murachelli AG, Confalonieri S, Magri L, Musacchio A, Di Fiore PP, Polo S, Schneider TR (2006) Crystal structure of the ubiquitin binding domains of rabex-5 reveals two modes of interaction with ubiquitin. Cell 124: 1183-95

Rieping W, Habeck M, Nilges M (2005) Inferential structure determination. Science 309: 303-6

Roberts RL, Barbieri MA, Ullrich J, Stahl PD (2000) Dynamics of rab5 activation in endocytosis and phagocytosis. J Leukoc Biol 68: 627-32

Robinson PJ, Trnka MJ, Pellarin R, Greenberg CH, Bushnell DA, Davis R, Burlingame AL, Sali A, Kornberg RD (2015) Molecular architecture of the yeast Mediator complex. Elife 4

Rojas AM, Fuentes G, Rausell A, Valencia A (2012) The Ras protein superfamily: evolutionary tree and role of conserved amino acids. J Cell Biol 196: 189-201

Russel D, Lasker K, Webb B, Velazquez-Muriel J, Tjioe E, Schneidman-Duhovny D, Peterson B, Sali A (2012) Putting the pieces together: integrative modeling platform software for structure determination of macromolecular assemblies. PLoS Biol 10: e1001244

Sali A, Blundell TL (1993) Comparative protein modelling by satisfaction of spatial restraints. J Mol Biol 234: 779-815

Shen MY, Sali A (2006) Statistical potential for assessment and prediction of protein structures. Protein Sci 15: 2507-24

Shih TY, Papageorge AG, Stokes PE, Weeks MO, Scolnick EM (1980) Guanine nucleotide-binding and autophosphorylating activities associated with the p21src protein of Harvey murine sarcoma virus. Nature 287: 686-91

Sondermann H, Soisson SM, Boykevisch S, Yang SS, Bar-Sagi D, Kuriyan J (2004) Structural analysis of autoinhibition in the Ras activator Son of sevenless. Cell 119: 393-405

Sonnichsen B, De Renzis S, Nielsen E, Rietdorf J, Zerial M (2000) Distinct membrane domains on endosomes in the recycling pathway visualized by multicolor imaging of Rab4, Rab5, and Rab11. J Cell Biol 149: 901-14

Sorkin A, McClure M, Huang F, Carter R (2000) Interaction of EGF receptor and grb2 in living cells visualized by fluorescence resonance energy transfer (FRET) microscopy. Curr Biol 10: 1395-8

Stenmark H, Vitale G, Ullrich O, Zerial M (1995) Rabaptin-5 is a direct effector of the small GTPase Rab5 in endocytic membrane fusion. Cell 83: 423-32

Villasenor R, Nonaka H, Del Conte-Zerial P, Kalaidzidis Y, Zerial M (2015) Regulation of EGFR signal transduction by analogue-to-digital conversion in endosomes. Elife 4

Walters BT, Ricciuti A, Mayne L, Englander SW (2012) Minimizing back exchange in the hydrogen exchange-mass spectrometry experiment. J Am Soc Mass Spectrom 23: 2132-9

Wittinghofer A, Vetter IR (2011) Structure-function relationships of the G domain, a canonical switch motif. Annu Rev Biochem 80: 943-71

Yadav KK, Bar-Sagi D (2010) Allosteric gating of Son of sevenless activity by the histone domain. Proc Natl Acad Sci U S A 107: 3436-40

Zerial M, McBride H (2001) Rab proteins as membrane organizers. Nat Rev Mol Cell Biol 2: 107-17

Zhang Z, Zhang T, Wang S, Gong Z, Tang C, Chen J, Ding J (2014) Molecular mechanism for Rabex-5 GEF activation by Rabaptin-5. Elife 3

Zhu G, Zhai P, Liu J, Terzyan S, Li G, Zhang XC (2004) Structural basis of Rab5-Rabaptin5 interaction in endocytosis. Nat Struct Mol Biol 11: 975-83

Figures

Figure 1: Rabex5 XL-MS Data and Structural Model

A

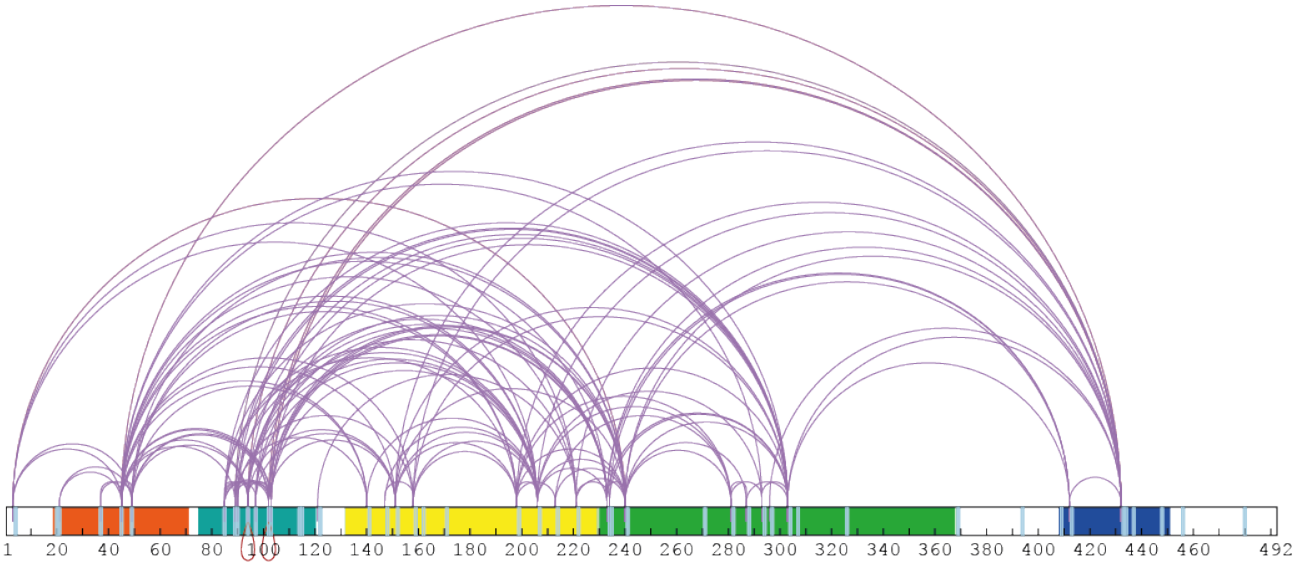

B

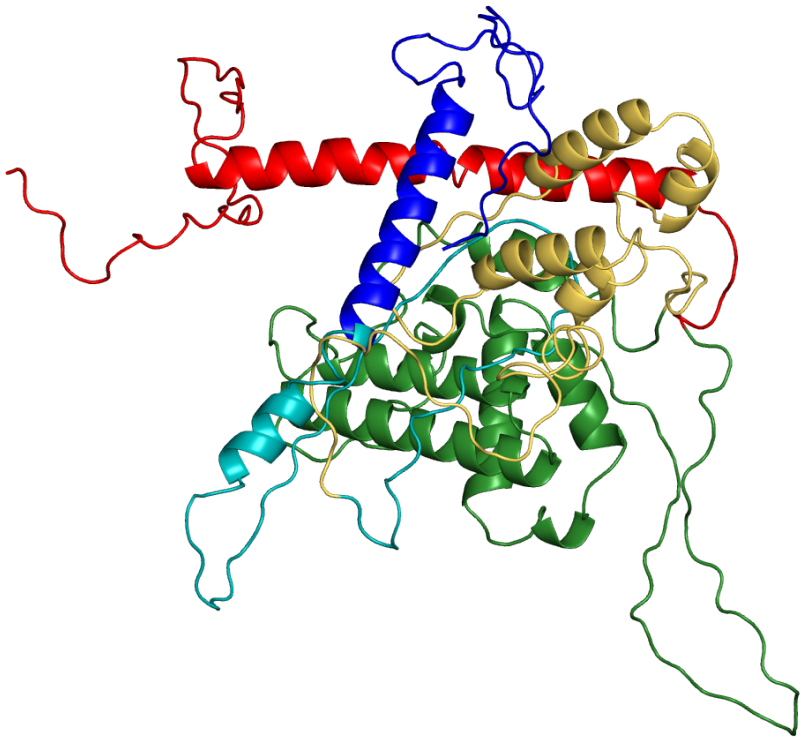

Figure 2: Domain Deletion Mutants

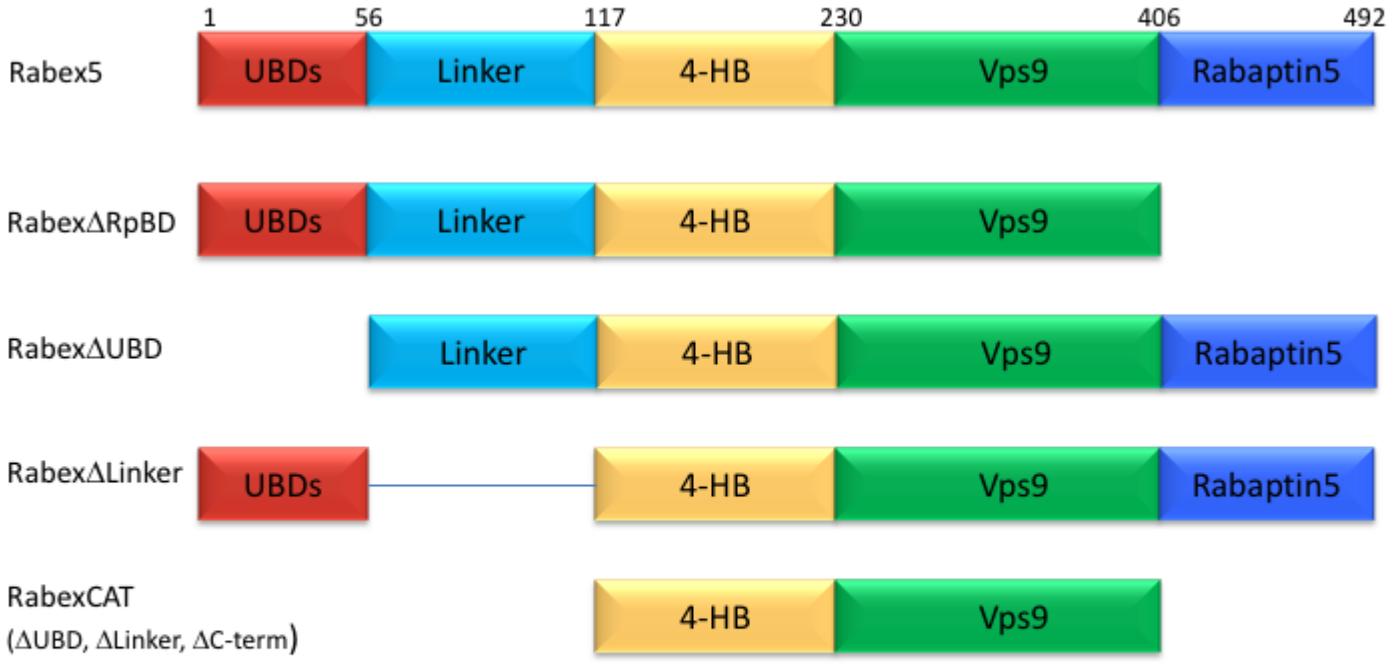

Figure 3: Rabex5 Nucleotide Exchange Kinetics

A

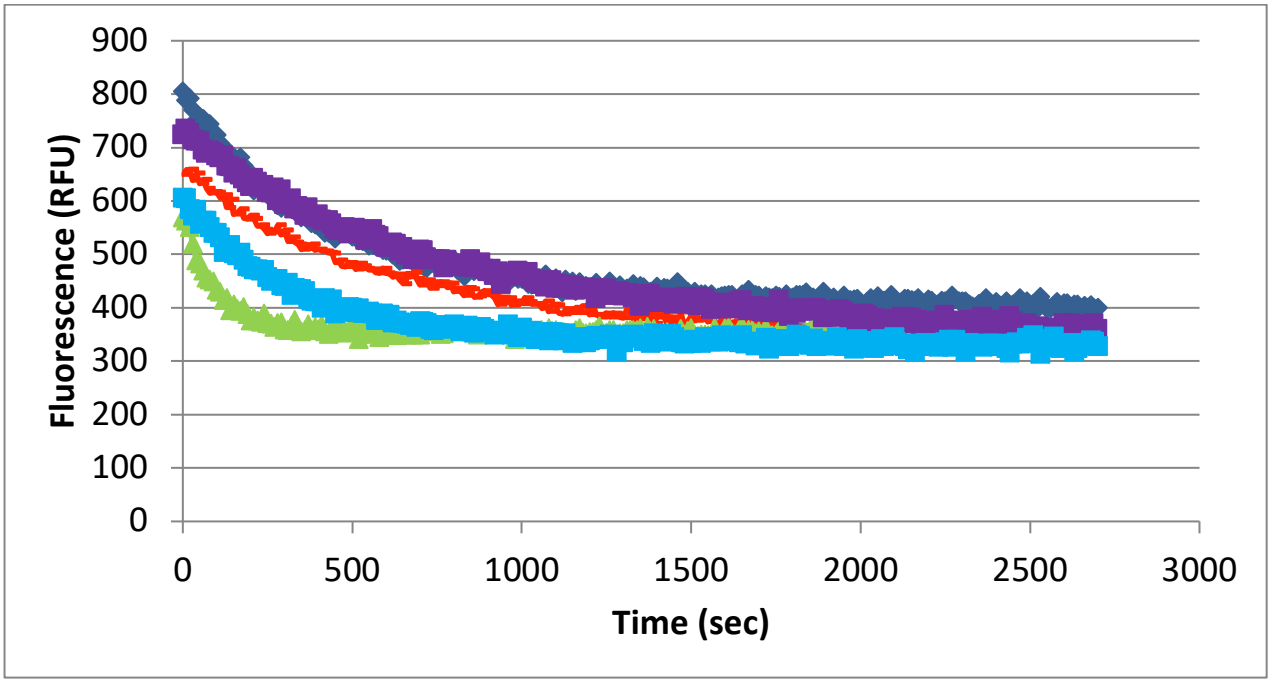

B

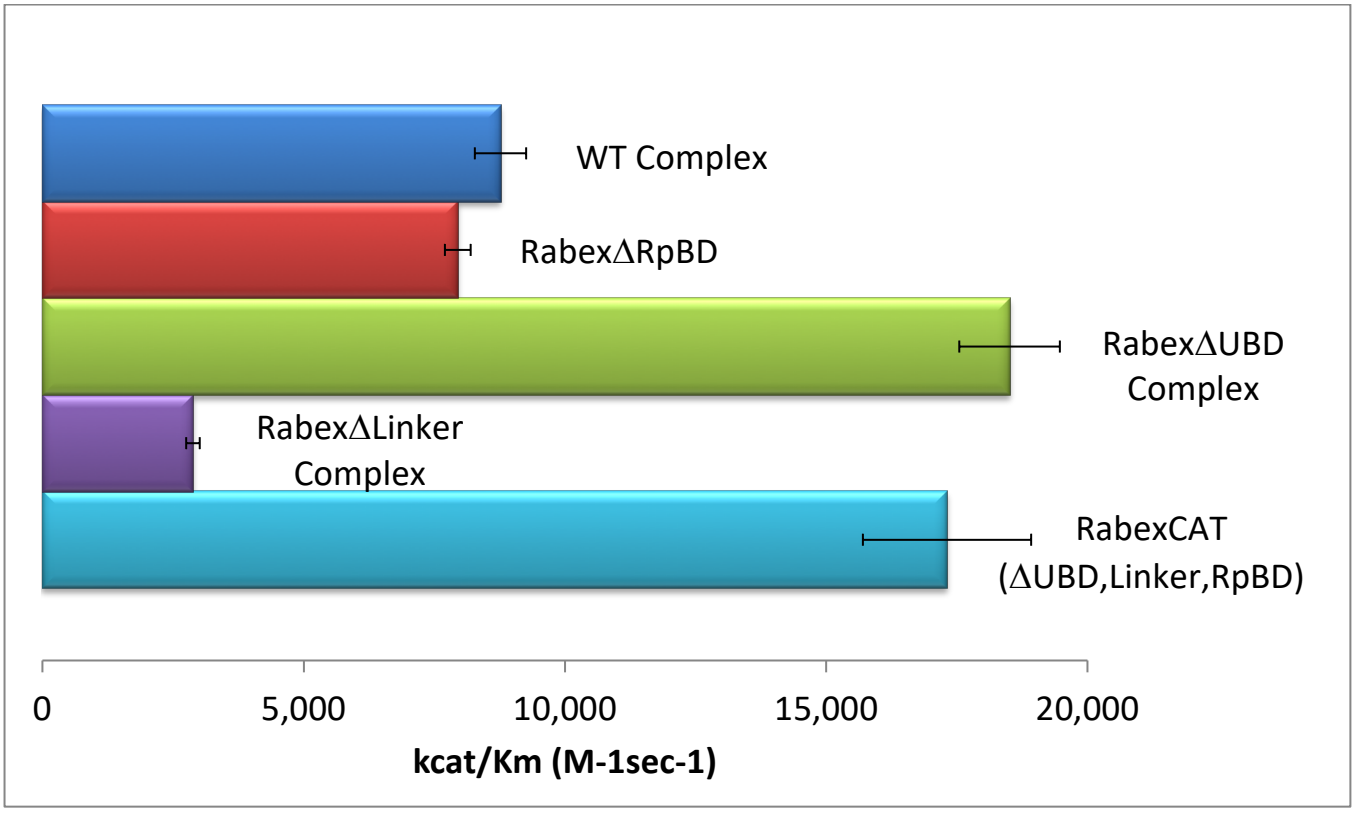

Figure 4: HDX-MS Data

Figure 4A: WT Rabex5 vs Rabex5:Rabaptin5 Complex

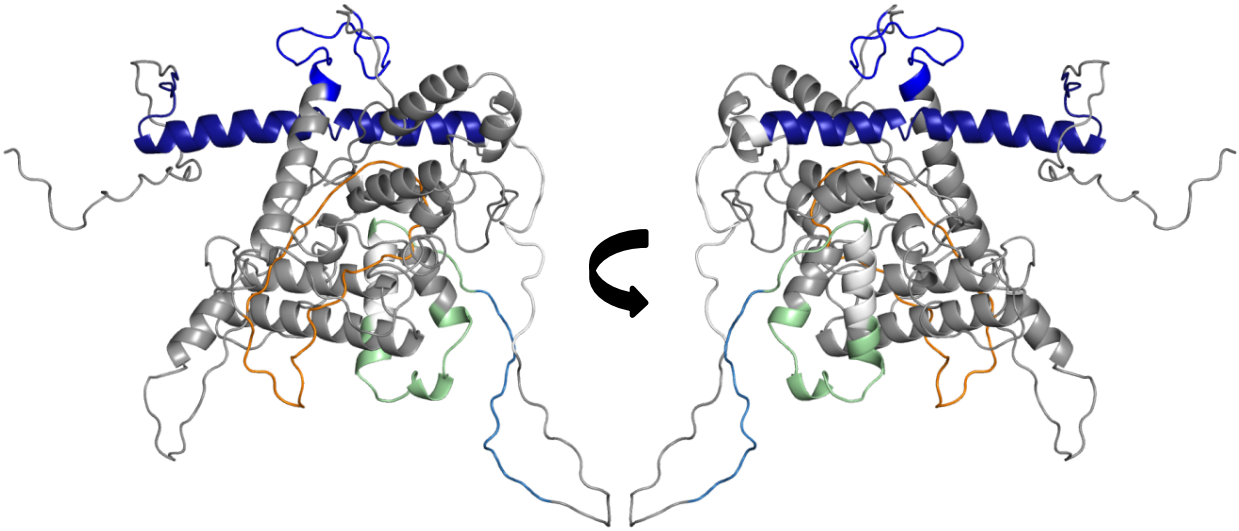

Figure 4B: WT Rabex5 vs RabexΔRpBD

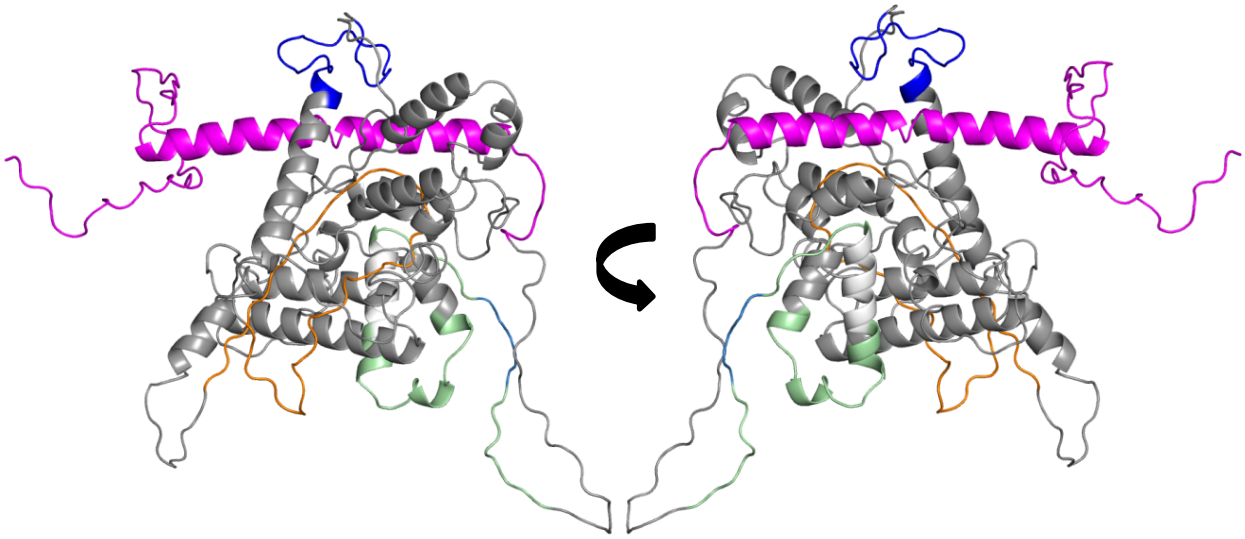

Figure 4C: WT Rabex5:Rabaptin5 Complex vs RabexΔUBD:Rabaptin5 Complex

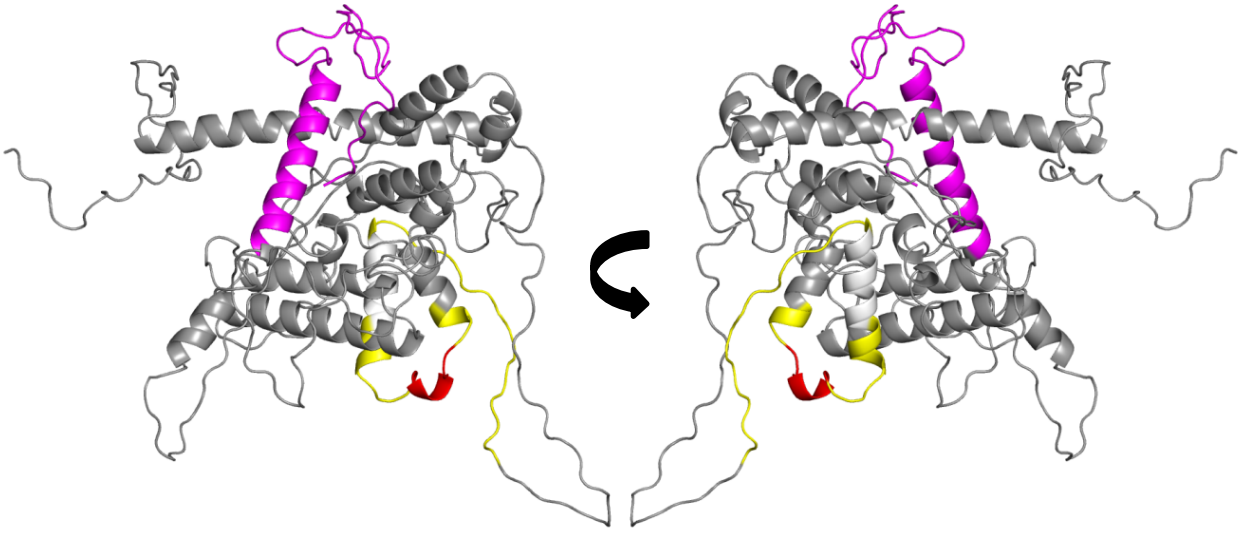

Figure 4D: WT Rabex5:Rabaptin5 Complex vs RabexΔLinker:Rabaptin5 Complex

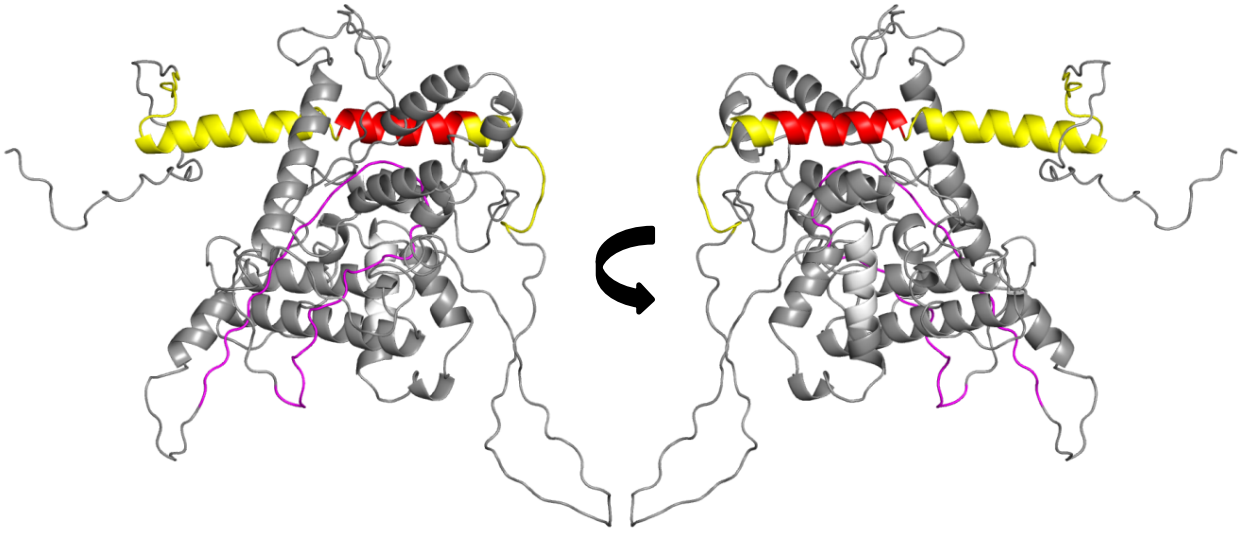

Figure 5: Effects of tetraUb on Nucleotide Exchange

A

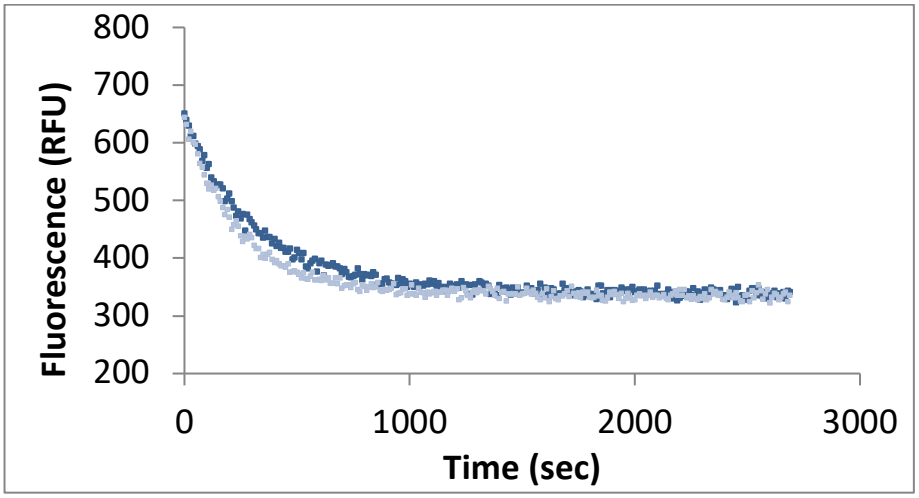

B

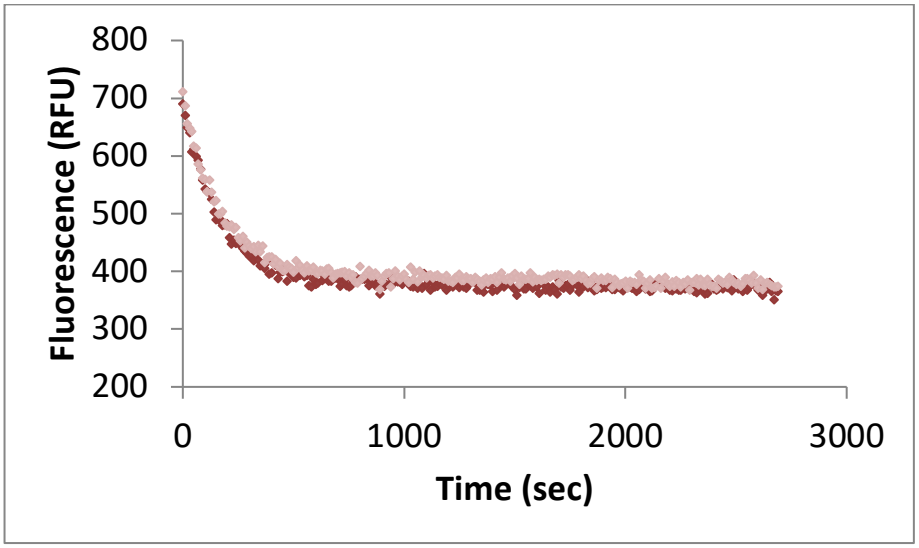

C

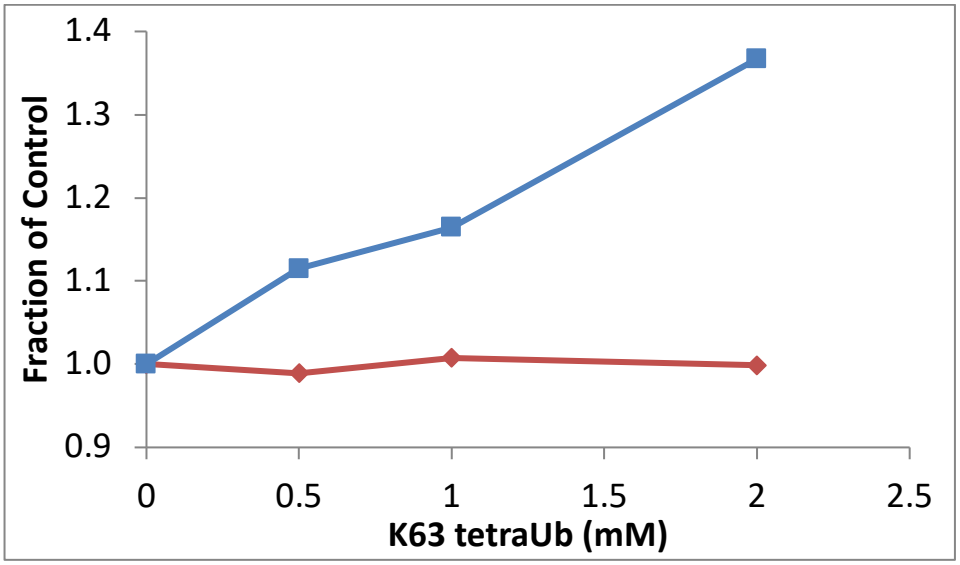

Figure 6: HDX-MS Results During Nucleotide Exchange

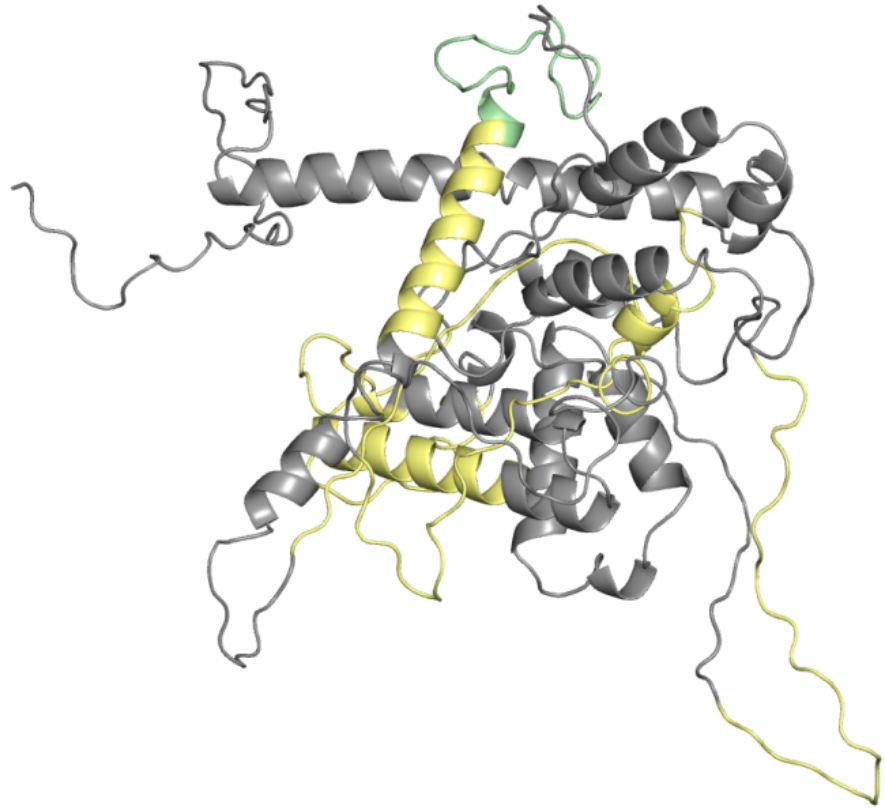

Figure 7: Peptide Profiles During Nucleotide Exchange

Total ion current and centroid spectra for a peptide corresponding to Rabex5 (83-120) in the presence (B and D) or absence of GTPγS (A and C) after 60s (A and B) or 300s (C and D) of deuterium uptake. Note the disappearance of signal at 60s upon addition of GTPγS and partial recovery at 300s.

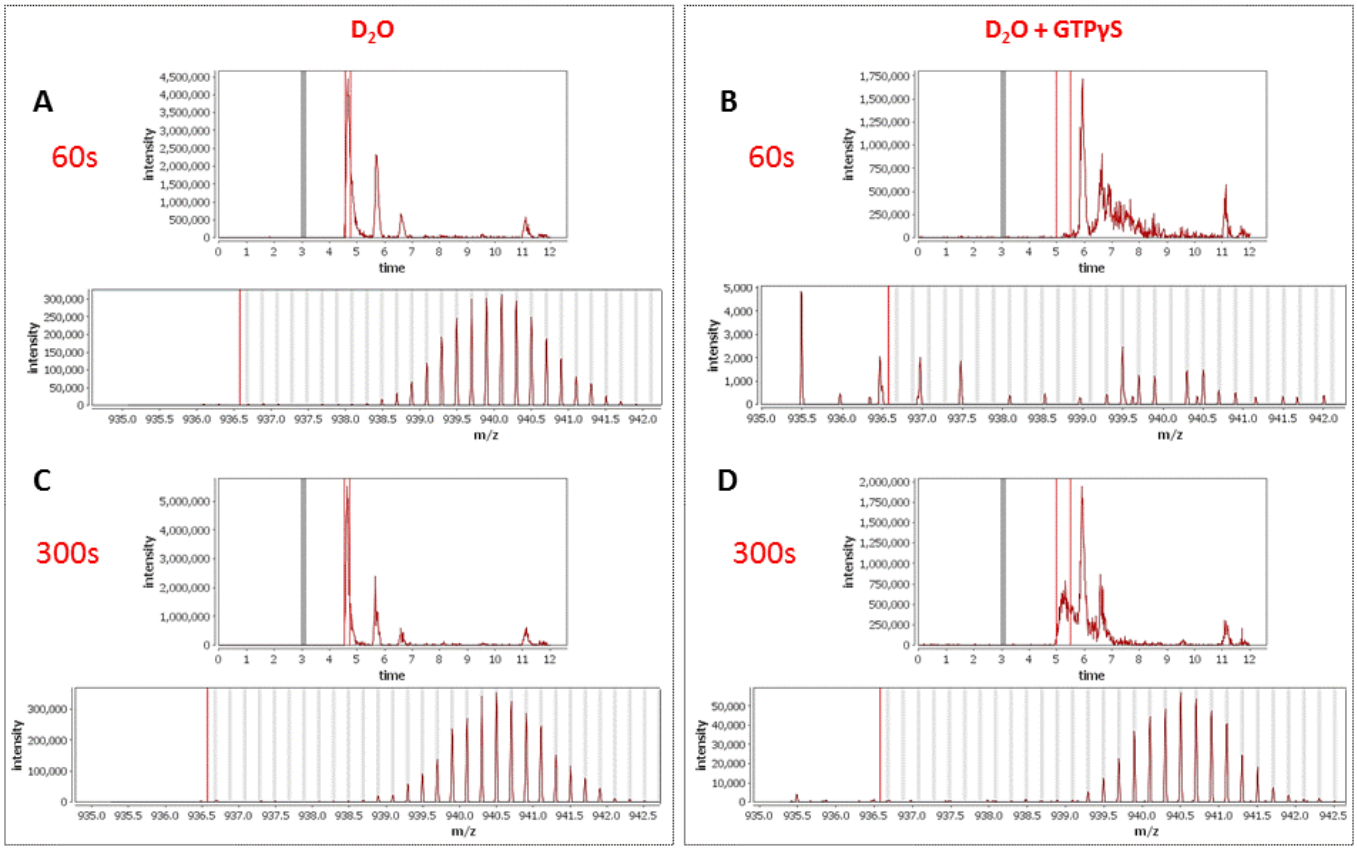

Supplementary
Table S1

				Top scoring model		Model with max XL satisfied		Total XL satisfied in cluster	
	4-HB, Vps9 Rotation	RpBD Positioning	#Cluster	Satisfied XL	Fraction	Satisfied XL	Fraction	Satisfied XL	Fraction
4q9u	rigid	rigid	#Cluster 0	106	0.87	107	0.88	107	0.88
4q9u	rigid	rigid	#Cluster 1	105	0.86	107	0.88	107	0.88
4q9u	rigid	rigid	#Cluster 2	104	0.85	107	0.88	107	0.88
4q9u	flexible	rigid	#Cluster 0	114	0.93	116	0.95	120	0.98
4q9u	flexible	rigid	#Cluster 1	113	0.93	119	0.98	121	0.99
4q9u	flexible	rigid	#Cluster 2	112	0.92	116	0.95	119	0.98
4q9u	rigid	flexible	#Cluster 0	107	0.88	109	0.89	115	0.94
4q9u	rigid	flexible	#Cluster 1	108	0.89	109	0.89	116	0.95
4q9u	rigid	flexible	#Cluster 2	103	0.84	106	0.87	107	0.88
4q9u	flexible	flexible	#Cluster 0	116	0.95	119	0.98	121	0.99
4q9u	flexible	flexible	#Cluster 1	115	0.94	119	0.98	121	0.99
4q9u	flexible	flexible	#Cluster 2	118	0.97	119	0.98	120	0.98
4n3z	rigid	rigid	#Cluster 0	109	0.89	110	0.90	112	0.92
4n3z	rigid	rigid	#Cluster 1	109	0.89	110	0.90	111	0.91
4n3z	rigid	rigid	#Cluster 2	108	0.89	111	0.91	111	0.91
4n3z	flexible	rigid	#Cluster 0	116	0.95	117	0.96	118	0.97
4n3z	flexible	rigid	#Cluster 1	116	0.95	117	0.96	118	0.97
4n3z	flexible	rigid	#Cluster 2	114	0.93	117	0.96	117	0.96
4n3z	rigid	flexible	#Cluster 0	108	0.89	109	0.89	109	0.89
4n3z	rigid	flexible	#Cluster 1	107	0.88	109	0.89	109	0.89
4n3z	rigid	flexible	#Cluster 2	107	0.88	109	0.89	110	0.90
4n3z	flexible	flexible	#Cluster 0	115	0.94	116	0.95	121	0.99
4n3z	flexible	flexible	#Cluster 1	111	0.91	117	0.96	119	0.98
4n3z	flexible	flexible	#Cluster 2	114	0.93	117	0.96	118	0.97

S1: HDX-MS Results

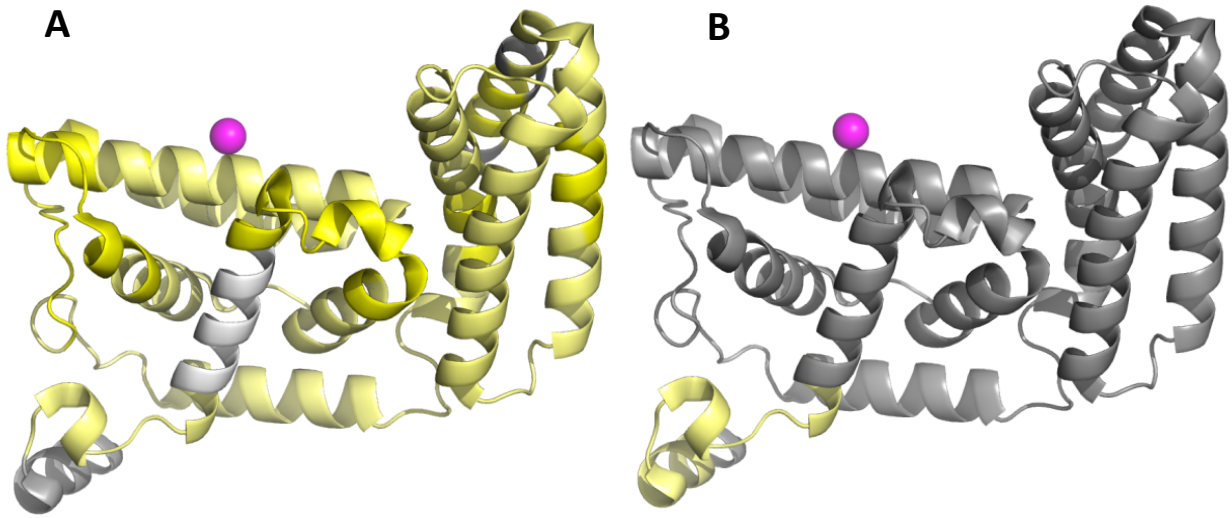

S2: Nucleotide Exchange Kinetics

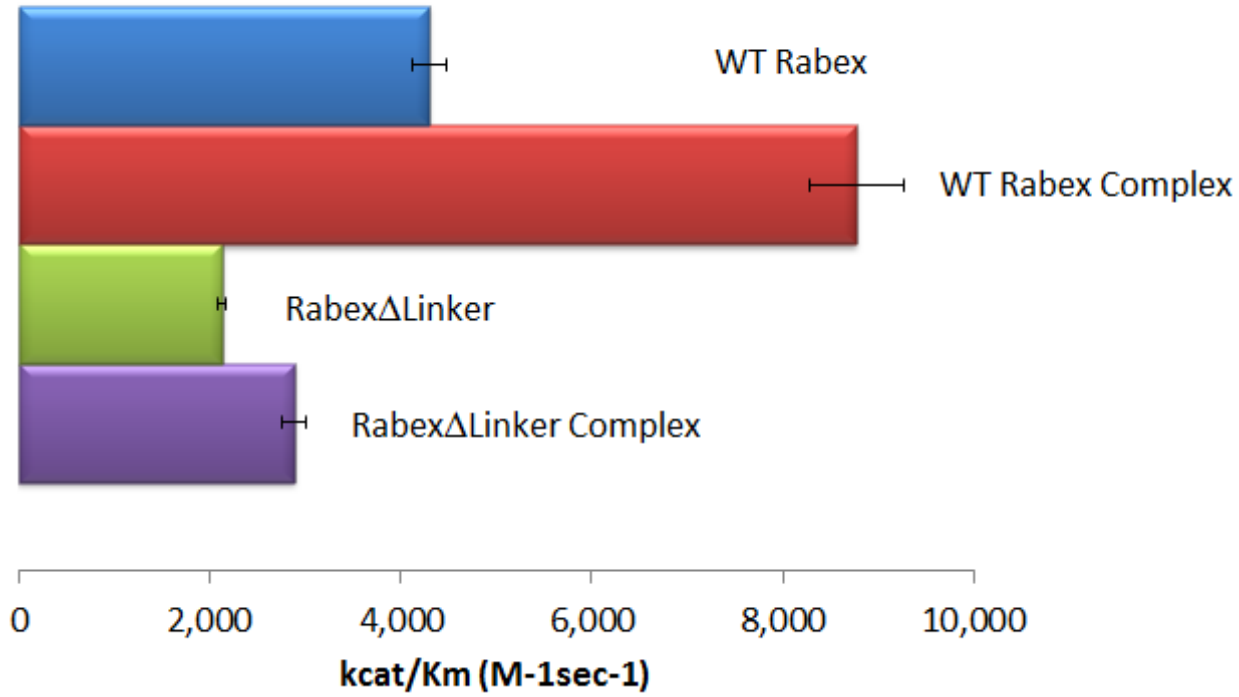

S4: 10s Deuterium Uptake in Rabex5

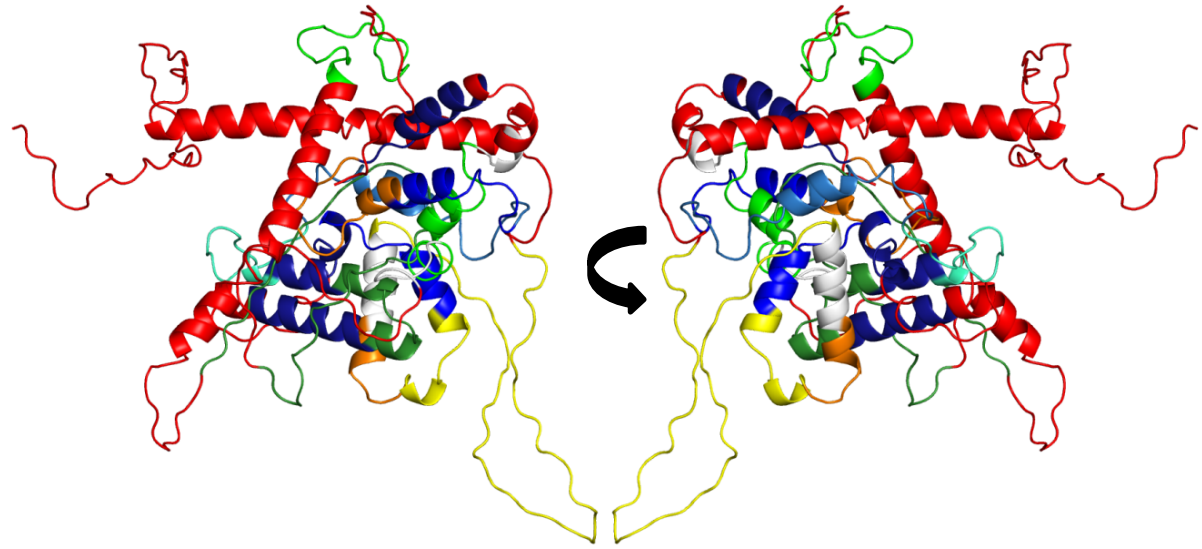

S5: HDX-MS Data Used to Generate Models

Rabex5 Binding to Rabaptin5 (Figure 4a)

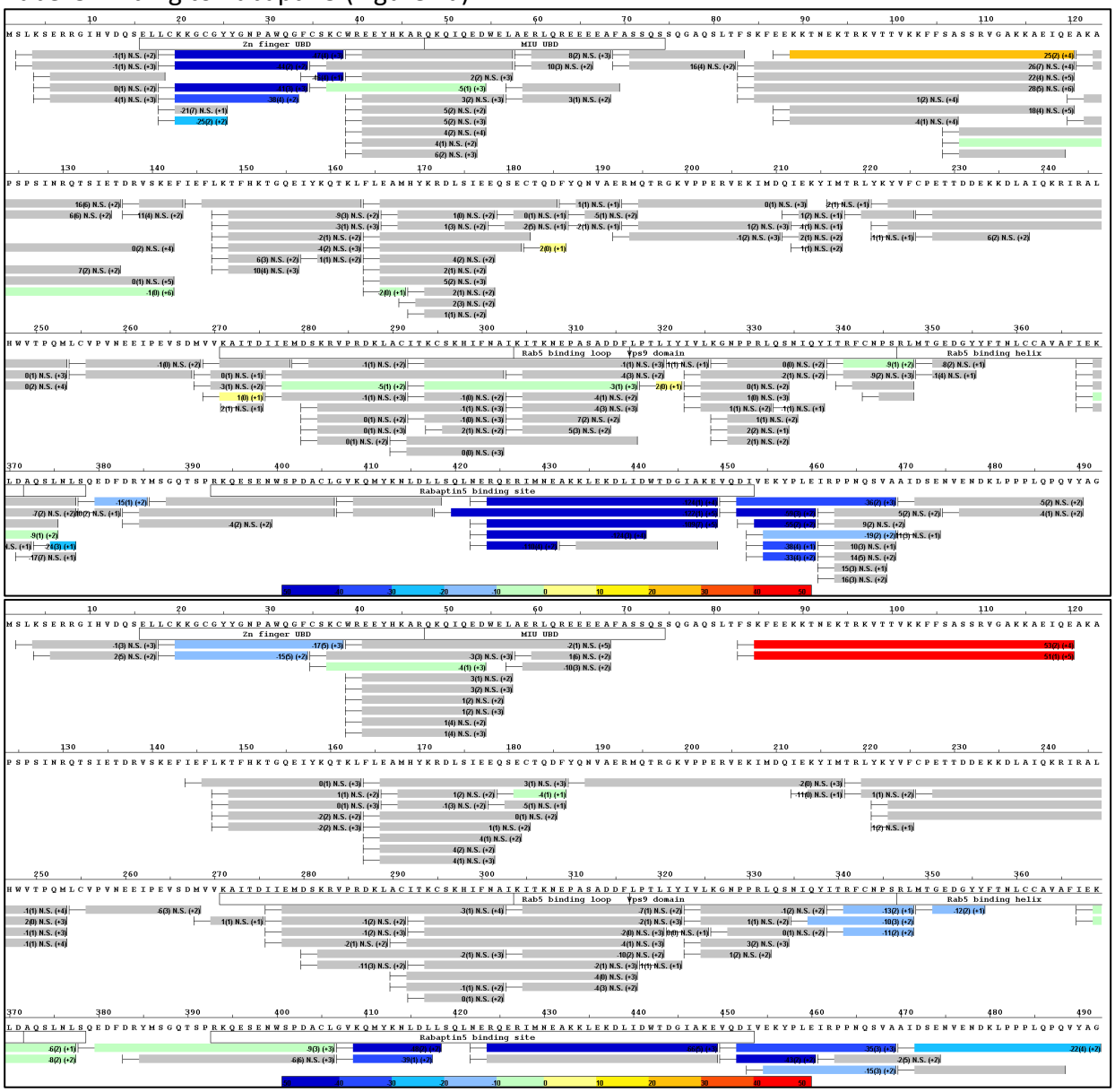

WT vs ΔRBD (Figure 4b)

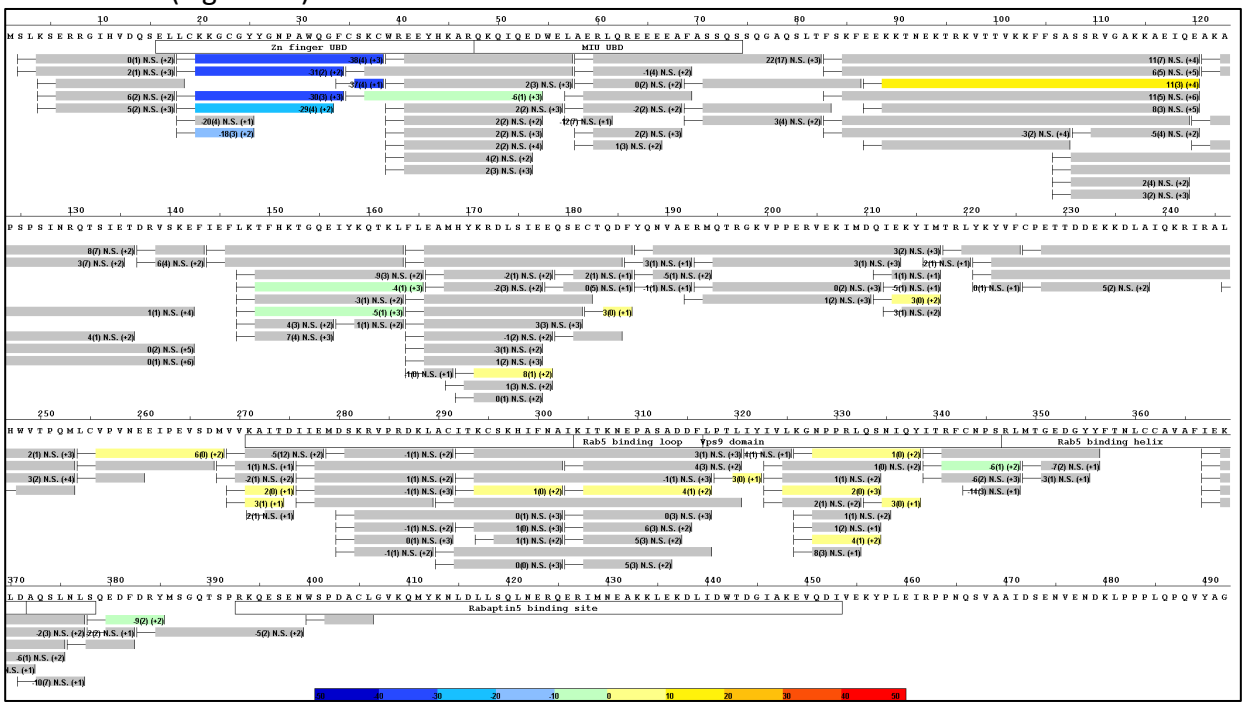

WT Complex vs RabexΔUBD Complex (Figure 4c)

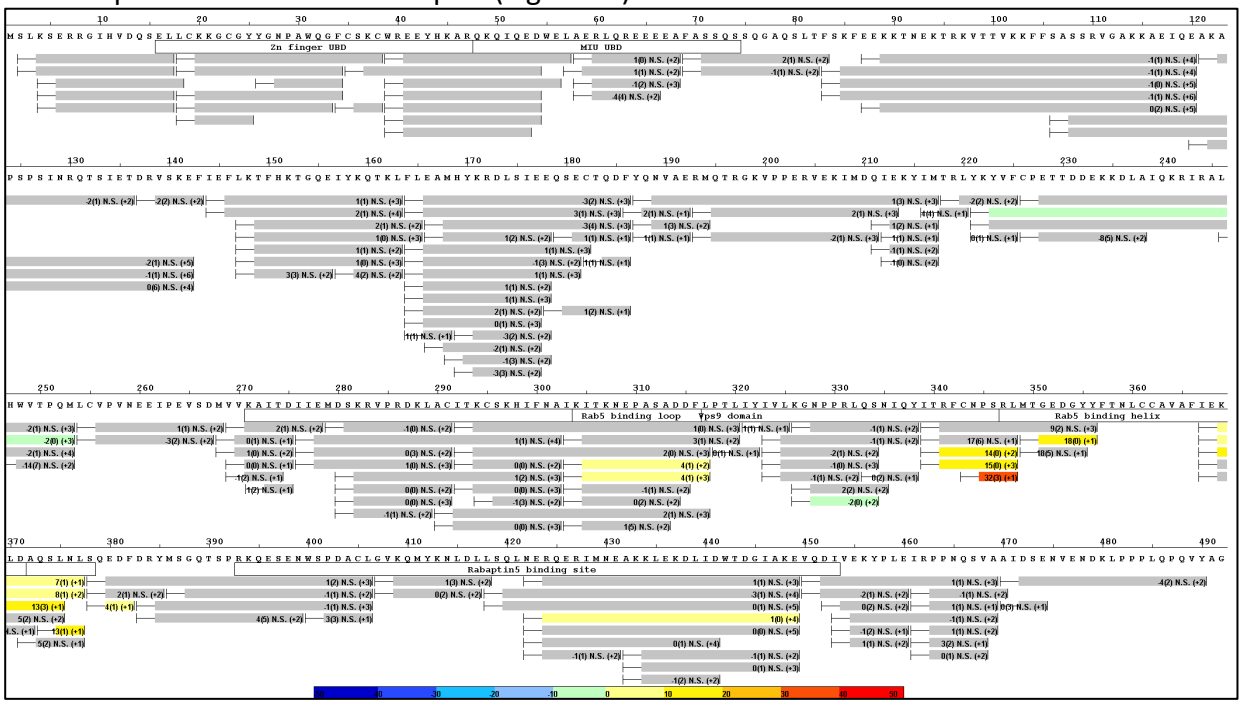

WT Complex vs RabexΔLinker Complex (Figure 4d)

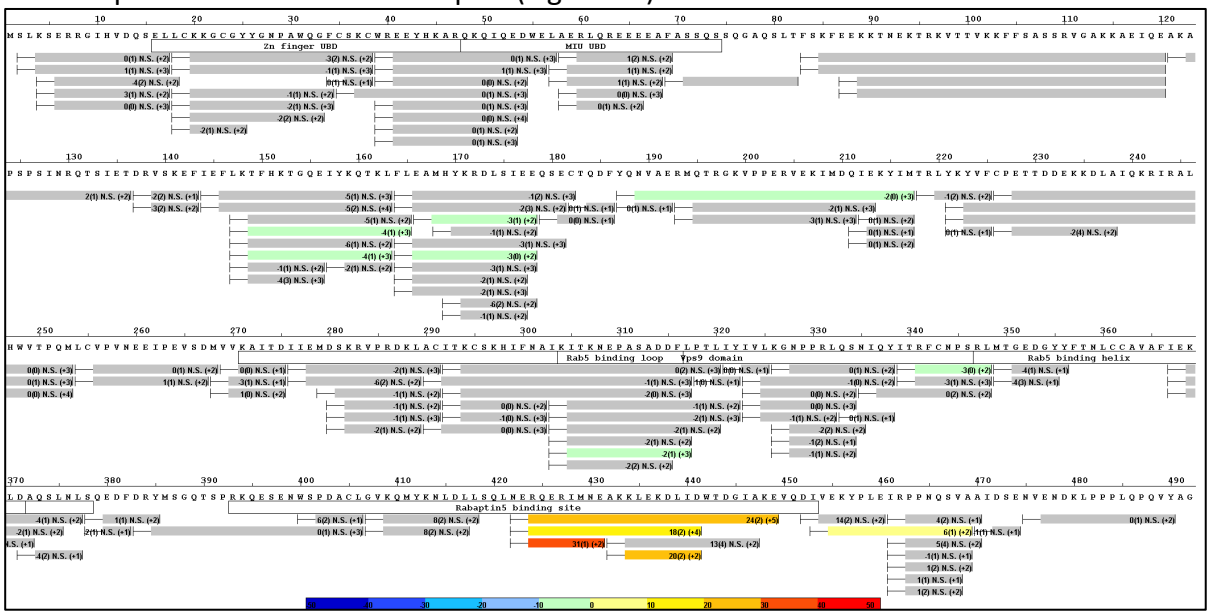

Nucleotide Exchange Reaction (Figure 6)

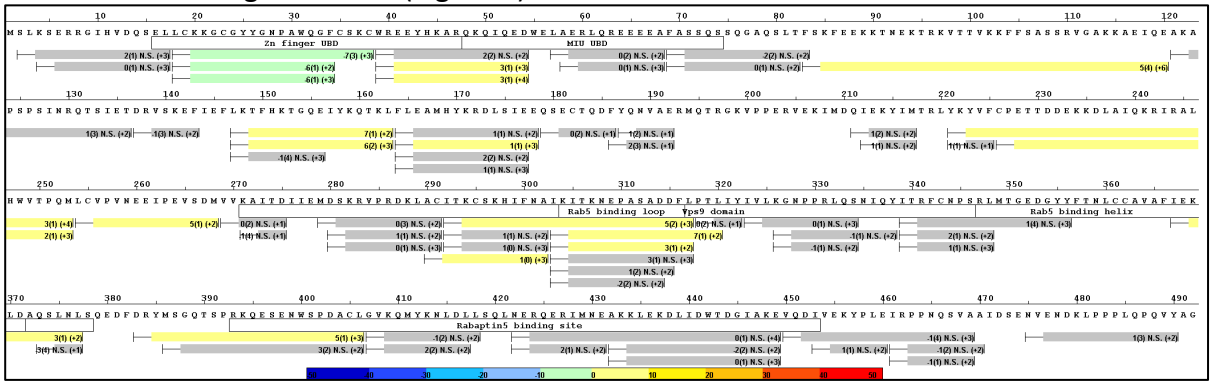

Rabex1-492 vs Rabex132-394 (Fig S1a)

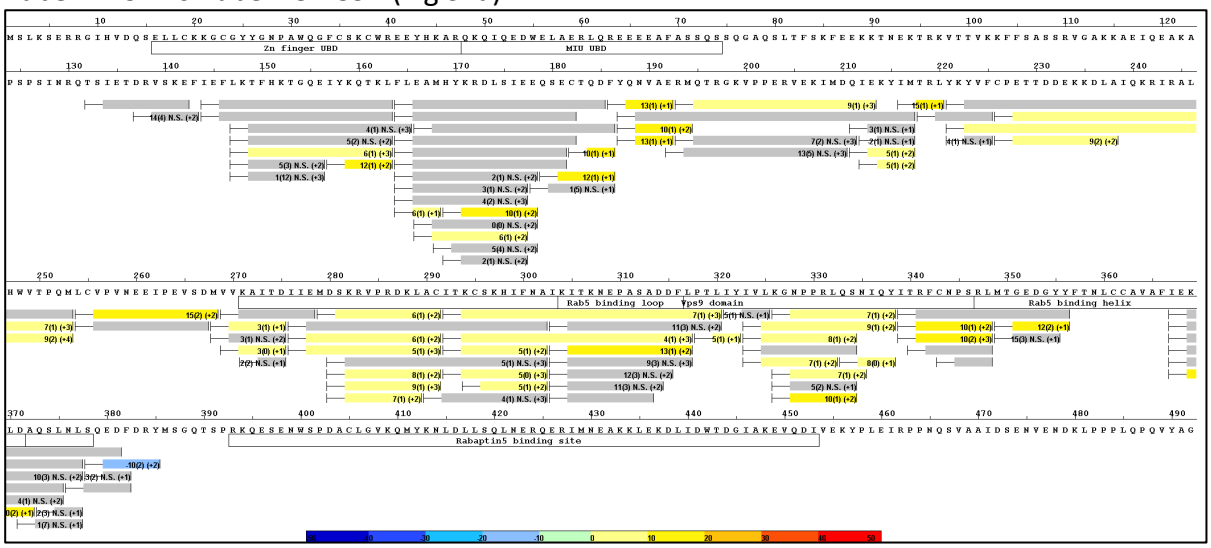

Rabex132-394 vs RabexCAT (Fig S1b)